analysis, the variant allele in the grandmother must have been transmitted by her father, and that in the mother must have been transmitted by her mother. The results indicated that the variant allele could be either methylated or unmethylated during gametogenesis, strongly suggesting no relation between the variants and ICR1-GOM. On the other hand, bisulfite sequencing including the 2,023,018C>T variant revealed that both the variant and wild-type alleles were heavily methylated in the patient (Fig. 1e), while differential methylation was maintained in other family members and normal controls without the variant (Fig. S2a). As the *de novo* variant on the maternal allele was located within the OCT-binding site, which is required for the maintenance of the unmethylated status in a mouse model, the variant was likely involved in ICR1-GOM (17, 18).

Finally, we performed EMSA to determine if 2,023,018C>T influenced the binding ability of nuclear protein factors, such as OCT4 and SOX2 (Fig. 2c). The wild-type probe formed two complexes (A and B) with the nuclear extracts of mouse ES cells and HEK293 cells expressing OCT4/SOX2 (lanes 2 and 3), whereas such complexes were not observed in the mutant probe (lanes 11 and 12). Complexes A and B competed more efficiently with wild-type than with the mutant competitor (lanes 4 to 7). Furthermore, complex B, but not A, was supershifted with the antibody against OCT4 (lane 8). The supershift did not occur with the antibody against SOX2 and with both antibodies using the mutant probe (lanes 9, 13, and 14). These data demonstrated that 2,023,018C>T abrogated binding ability of a nuclear factor, most likely OCT4. Taken together, our data strongly suggest that 2,023,018C>T is a mutation that could prevent OCT4 binding to the OCT-binding site and induce ICR1-GOM, leading to BWS.

Discussion

We identified a novel *de novo* point mutation, chr11: 2,023,018C>T, in OCT-binding site 1 within repeat A2 in a BWS patient with ICR1-GOM. Our data strongly suggest the involvement of the mutation in GOM at ICR1. In a mouse cell model, the evolutionarily well-conserved dyad octamer motif within ICR1, which is bound by OCT protein, has been shown to be required for the maintenance of unmethylated status competing against *de novo* methylation (17). In addition, the importance of a SOX motif flanked by an OCT motif has also been reported (19). Recent studies have shown that the SOX–OCT motif functions to maintain unmethylated status *in vitro* and *in vivo*; a cooperative function of CTCF and OCT/SOX for maintenance of differential methylation has been suggested as responsible (18, 19). Although there is one OCT-binding site in mice, three evolutionarily conserved OCT-binding sites (0, 1, 2) are located in and around ICR1 in humans. As all mutations and the small deletion previously reported in addition to our case occurred in site 1 within repeat A2 (Fig. 1a), site 1 within repeat A2 likely plays a more important role for maintaining unmethylated status of maternal ICR1 in humans than the other OCT-binding sites (10, 12, 13).

ICR1-GOM cases, including ours, with mutations/deletions also show partial hypermethylation in spite of pre-existent genetic aberrations in the oocyte (9, 12, 13, 20), suggesting aberrant hypermethylation at ICR1 would also be stochastically acquired at a cellular level even in the existence of such aberrations.

As for SRS, including familial cases, the ICR1 mutation has not been found except in one sporadic case to date (10). We did not find any promising mutations in this study, suggesting the cause of ICR1 methylation defects to differ between SRS and BWS.

In conclusion, we identified a novel *de novo* point mutation of OCT-binding site 1 within repeat A2, a location suggested to play an important role for maintaining the unmethylated status of maternal ICR1 in humans, on the maternal allele in a BWS patient with ICR1-GOM. However, genetic aberrations of ICR1 explain only 20% of BWS cases with ICR1-GOM (10). As aberrant methylation may occur as a consequence of stochastic events or environmental influences irrespective of ICR1 mutations, unknown causes for ICR1 methylation defects should be clarified.

Supporting Information

The following Supporting information is available for this article:

Fig. S1. EMSA for all variants found in this study, except for those in BWS-047 and BWS-s061, using the nuclear extract from mouse ES cells. The variant in BWS-s081 was located outside of ICR1, and a CpG site within the probe sequence was mostly unmethylated in three normal controls (data not shown). Thus, an unmethylated probe was used for it. Since the variants in BWS-s100 and SRS-s03 were located 3′ of CTS6 and found on the maternal allele, unmethylated probes were used for them. As for the variant in SRS-002, it was located 5′ of CTS1 but its parental origin was unknown. Thus, both unmethylated and methylated probes were used for it. There was no difference between a wt-probe and a variant-probe in each variant except for the BWS-s043 mutation. A wt-probe for the BWS-s043 mutation formed two complexes, whereas such complexes were not observed with a probe for the mutation. These results suggested that only the BWS-s043 mutation affected the protein–DNA interaction (see text and Fig. 2c for details). WT, probe for the wild-type sequence; MUT, probe for the BWS-s043 mutation; VAR, probe for the variant sequence; um, unmethylated probe; me, methylated probe; mES NE, nuclear extract from mouse ES cells.
Fig. S2. Bisulfite sequencing of the region encompassing the 2,023,018 variant, CTS1, and CTS4. (**a**) Results for the 2,023,018 variant. In the healthy members of the BWS-s043 family, comprised of the maternal grandmother, mother, and father, showed differential methylation. Three normal controls also showed differential methylation. In particular, normal control 3 was heterozygous for a SNP (rs61520309) and showed differential methylation in an allele-dependent manner. Open and filled circles indicate unmethylated and methylated CpG sites, respectively. (**b**) Results for CTS1. Two normal controls that were heterozygous for a SNP (rs2525885) showed differential methylation. The healthy family members also showed differential methylation, whereas the patient, BWS-s043, showed aberrant hypermethylation. CpG sites within CTS1 are indicated by a short horizontal line. X indicates T of the SNP (rs2525885). (**c**) Results for CTS4. The healthy family members and two normal controls showed differential

methylation. Among them, the parents and two normal controls were heterozygous for a SNP (rs2525883). The patient, BWS-s043, showed aberrant hypermethylation. CpG sites within CTS4 were indicated by a short horizontal line. X indicates T of the SNP (rs2525883).
Table S1. PCR primers and oligonucleotide probes used in this study.

Additional Supporting information may be found in the online version of this article.

Acknowledgements

This study was supported, in part, by a Grant for Research on Intractable Diseases from the Ministry of Health, Labor, and Welfare; a Grant for Child Health and Development from the National Center for Child Health and Development; a Grant-in-Aid for Challenging Exploratory Research; and, a Grant-in-Aid for Scientific Research (C) from the Japan Society for the Promotion of Science.

References

1. Weksberg R, Shuman C, Beckwith JB. Beckwith–Wiedemann syndrome. Eur J Hum Genet 2010: 18: 8–14.
2. Gicquel C, Rossignol S, Cabrol S et al. Epimutation of the telomeric imprinting center region on chromosome 11p15 in Silver–Russell syndrome. Nat Genet 2005: 37: 1003–1007.
3. Bell AC, Felsenfeld G. Methylation of a CTCF-dependent boundary controls imprinted expression of the Igf2 gene. Nature 2000: 405: 482–485.
4. Hark AT, Schoenherr CJ, Katz DJ, Ingram RS, Levorse JM, Tilghman SM. CTCF mediates methylation-sensitive enhancer-blocking activity at the H19/Igf2 locus. Nature 2000: 405: 486–489.
5. Schoenherr CJ, Levorse JM, Tilghman SM. CTCF maintains differential methylation at the Igf2/H19 locus. Nat Genet 2003: 33: 66–69.
6. Pant V, Mariano P, Kanduri C et al. The nucleotides responsible for the direct physical contact between the chromatin insulator protein CTCF and the H19 imprinting control region manifest parent of origin-specific long-distance insulation and methylation-free domains. Genes Dev 2003: 17: 586–590.
7. Sparago A, Cerrato F, Vernucci M, Ferrero GB, Silengo MC, Riccio A. Microdeletions in the human H19 DMR result in loss of IGF2 imprinting and Beckwith–Wiedemann syndrome. Nat Genet 2004: 36: 958–960.
8. Prawitt D, Enklaar T, Gärtner-Rupprecht B et al. Microdeletion of target sites for insulator protein CTCF in a chromosome 11p15 imprinting center in Beckwith–Wiedemann syndrome and Wilms' tumor. Proc Natl Acad Sci U S A 2005: 102: 4085–4090.
9. Beygo J, Citro V, Sparago A et al. The molecular function and clinical phenotype of partial deletions of the IGF2/H19 imprinting control region depends on the spatial arrangement of the remaining CTCF-binding sites. Hum Mol Genet 2013: 22: 544–557.
10. Demars J, Shmela ME, Rossignol S et al. Analysis of the IGF2/H19 imprinting control region uncovers new genetic defects, including mutations of OCT-binding sequences, in patients with 11p15 fetal growth disorders. Hum Mol Genet 2010: 19: 803–814.
11. Quenneville S, Verde G, Corsinotti A et al. In embryonic stem cells, ZFP57/KAP1 recognize a methylated hexanucleotide to affect chromatin and DNA methylation of imprinting control regions. Mol Cell 2011: 44: 361–372.
12. Poole RL, Docherty LE, Al Sayegh A et al. Targeted methylation testing of a patient cohort broadens the epigenetic and clinical description of imprinting disorders. Am J Med Genet A 2013: 161: 2174–2182.
13. Berland S, Appelbäck M, Bruland O et al. Evidence for anticipation in Beckwith–Wiedemann syndrome. Eur J Hum Genet 2013: 21: 1344–1348.
14. Higashimoto K, Nakabayashi K, Yatsuki H et al. Aberrant methylation of H19-DMR acquired after implantation was dissimilar in soma versus placenta of patients with Beckwith–Wiedemann syndrome. Am J Med Genet A 2012: 158A: 1670–1675.
15. Soejima H, Nakagawachi T, Zhao W et al. Silencing of imprinted CDKN1C gene expression is associated with loss of CpG and histone H3 lysine 9 methylation at DMR-LIT1 in esophageal cancer. Oncogene 2004: 23: 4380–4388.
16. Mackay DJ, Callaway JL, Marks SM et al. Hypomethylation of multiple imprinted loci in individuals with transient neonatal diabetes is associated with mutations in ZFP57. Nat Genet 2008: 40: 949–951.
17. Hori N, Nakano H, Takeuchi T et al. A dyad Oct-binding sequence functions as a maintenance sequence for the unmethylated state within the H19/Igf2-imprinted control region. J Biol Chem 2002: 277: 27960–27967.
18. Sakaguchi R, Okamura E, Matsuzaki H, Fukamizu A, Tanimoto K. Sox-Oct motifs contribute to maintenance of the unmethylated H19 ICR in YAC transgenic mice. Hum Mol Genet 2013: 22: 4627–4637.
19. Hori N, Yamane M, Kouno K, Sato K. Induction of DNA demethylation depending on two sets of Sox2 and adjacent Oct3/4 binding sites (Sox-Oct motifs) within the mouse H19/insulin-like growth factor 2 (Igf2) imprinted control region. J Biol Chem 2012: 287: 44006–44016.
20. Sparago A, Russo S, Cerrato F et al. Mechanisms causing imprinting defects in familial Beckwith–Wiedemann syndrome with Wilms' tumour. Hum Mol Genet 2007: 16: 254–264.

Clinical Endocrinology (2013) doi: 10.1111/cen.12379

ORIGINAL ARTICLE

IMAGe syndrome: clinical and genetic implications based on investigations in three Japanese patients

Fumiko Kato*, Takashi Hamajima†, Tomonobu Hasegawa‡, Naoko Amano‡, Reiko Horikawa§, Gen Nishimura¶, Shinichi Nakashima*, Tomoko Fuke**, Shinichirou Sano**, Maki Fukami** and Tsutomu Ogata*

*Department of Pediatrics, Hamamatsu University School of Medicine, Hamamatsu, †Division of Endocrinology and Metabolism, Aichi Children's Health and Medical Center, Obu, ‡Department of Pediatrics, Keio University School of Medicine, §Division of Endocrinology and Metabolism, National Center for Child Health and Development, Tokyo, ¶Department of Radiology, Tokyo Metropolitan Children's Medical Center, Fuchu, and **Department of Molecular Endocrinology, National Research Institute for Child Health and Development, Tokyo, Japan

Summary

Objective Arboleda *et al.* have recently shown that IMAGe (intra-uterine growth restriction, metaphyseal dysplasia, adrenal hypoplasia congenita and genital abnormalities) syndrome is caused by gain-of-function mutations of maternally expressed gene *CDKN1C* on chromosome 11p15.5. However, there is no other report describing clinical findings in patients with molecularly studied IMAGe syndrome. Here, we report clinical and molecular findings in Japanese patients.

Patients We studied a 46,XX patient aged 8·5 years (case 1) and two 46,XY patients aged 16·5 and 15·0 years (cases 2 and 3).

Results Clinical studies revealed not only IMAGe syndrome-compatible phenotypes in cases 1–3, but also hitherto undescribed findings including relative macrocephaly and apparently normal pituitary-gonadal endocrine function in cases 1–3, familial glucocorticoid deficiency (FGD)-like adrenal phenotype and the history of oligohydramnios in case 2, and arachnodactyly in case 3. Sequence analysis of *CDKN1C*, pyrosequencing-based methylation analysis of KvDMR1 and high-density oligonucleotide array comparative genome hybridization analysis for chromosome 11p15.5 were performed, showing an identical *de novo* and maternally inherited *CDKN1C* gain-of-function mutation (p.Asp274Asn) in cases 1 and 2, respectively, and no demonstrable abnormality in case 3.

Conclusions The results of cases 1 and 2 with *CDKN1C* mutation would argue the following: [1] relative macrocephaly is consistent with maternal expression of *CDKN1C* in most tissues and biparental expression of *CDKN1C* in the foetal brain; [2] FGD-like phenotype can result from *CDKN1C* mutation; and [3] genital abnormalities may primarily be ascribed to placental dysfunction. Furthermore, lack of *CDKN1C* mutation in case 3 implies genetic heterogeneity in IMAGe syndrome.

(Received 1 October 2013; returned for revision 24 November 2013; finally revised 26 November 2013; accepted 29 November 2013)

Correspondence: Dr. Tsutomu Ogata, Department of Pediatrics, Hamamatsu University School of Medicine, 1-20-1 Handayama, Higashi-ku, Hamamatsu 431-3192, Japan. Tel./Fax: +81 53 435 2310;
E-mail: tomogata@hama-med.ac.jp

Introduction

IMAGe syndrome is a multisystem developmental disorder named by the acronym of intra-uterine growth restriction (IUGR), metaphyseal dysplasia and adrenal hypoplasia congenita common to both 46,XY and 46,XX patients, and genital abnormalities specific to 46,XY patients.[1] In addition to these salient clinical features, hypercalciuria has been reported frequently in IMAGe syndrome.[1,2] This condition occurs not only as a sporadic form but also as a familial form.[1–3] Furthermore, transmission analysis in a large pedigree has revealed an absolute maternal inheritance of this condition, indicating the relevance of a maternally expressed gene to the development of IMAGe syndrome.[3]

Subsequently, Arboleda *et al.*[4] have mapped the causative gene to a ~17·2-Mb region on chromosome 11 by an identity-by-descent analysis in this large pedigree and performed targeted exon array capture and high-throughput genomic sequencing for this region in the affected family members and in other sporadic patients. Consequently, they have identified five different missense mutations in the maternally expressed gene *CDKN1C* (cyclin-dependent kinase inhibitor 1C) that resides on the imprinting control region 2 (ICR2) domain at chromosome 11p15.5 and encodes a negative regulator for cell proliferation.[4–6] Notably, all the missense mutations are clustered within a specific segment of PCNA-binding domain, and functional studies have implicated that these mutations have gain-of-function effects.[4] Thus, IMAGe syndrome appears to constitute a mirror image of Beckwith–Wiedemann syndrome (BWS) in terms of the

CDKN1C function, because multiple *CDKN1C* loss-of-function mutations have been identified in BWS with no mutation shared in common by IMAGe syndrome and BWS.[4,5]

However, several matters remain to be clarified in IMAGe syndrome, including phenotypic spectrum and underlying mechanism(s) for the development of each phenotype in *CDKN1C*-mutation-positive patients, and the presence or absence of genetic heterogeneity. Here, we report clinical and molecular findings in three patients with IMAGe syndrome and discuss these unresolved matters.

Patients and methods

Patients

We studied one previously described 46,XX patient (case 1)[7] and two hitherto unreported 46,XY patients (cases 2 and 3). In cases 1–3, no pathologic mutations were identified in the coding exons and their splice cites of *NR5A1* (*SF1*) and *NR0B1* (*DAX1*) relevant to adrenal hypoplasia,[8] and *MC2R*, *MRAP*, *STAR* and *NNT* involved in familial glucocorticoid deficiency (FGD).[9]

Ethical approval and samples

This study was approved by the Institutional Review Board Committee at Hamamatsu University School of Medicine. Molecular studies were performed using leucocyte genomic DNA samples of cases 1–3 and the parents of cases 1 and 2, after obtaining written informed consent.

Sequence analysis of CDKN1C

The coding exons 1 and 2 and their flanking splice sites were amplified by polymerase chain reaction (PCR) (Fig. 1a), using primers shown in Table S1. Subsequently, the PCR products were subjected to direct sequencing from both directions on ABI 3130 autosequencer (Life Technologies, Carlsbad, CA, USA). In this regard, if a nucleotide variation were present within the primer-binding site(s), this may cause a false-negative finding because of amplification failure of a mutation-positive allele. Thus, PNCA-binding domain was examined with different primer sets. To confirm a heterozygous mutation, the corresponding PCR products were subcloned with TOPO TA Cloning Kit (Life Technologies), and normal and mutant alleles were sequenced separately.

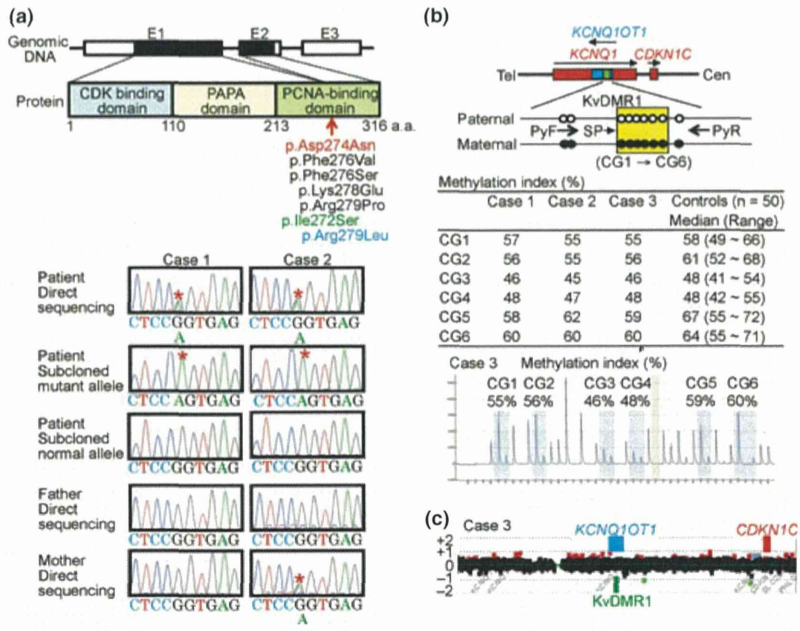

Fig. 1 Summary of molecular studies. (a) Sequence analysis of *CDKN1C*. *CDKN1C* consists of three exons (E1–E3), and the black and white boxes denote the coding regions and the untranslated regions, respectively. CDKN1C protein is composed of 316 amino acids and contains CDK binding domain, PAPA domain and PCNA-binding domain. The p.Asp274Asn mutation found in this study and the previous study[4] is shown in red. The four mutations written in black have also been identified in IMAGe syndrome.[4] The pIle272Ser mutation written in green has been detected in atypical IMAGe syndrome lacking skeletal lesion,[22] and the pArg279Leu mutation written in blue has been found in SRS.[24] Electrochromatograms denote a *de novo* p.Asp274Asn mutation in case 1 and a maternally inherited p.Asp274Asn mutation in case 2. (b) Methylation analysis of KvDMR1 at the ICR2 domain. The cytosine residues at the CpG dinucleotides are unmethylated after paternal transmission (open circles) and methylated after maternal transmission (filled circles). *KCNQ1OT1* is a paternally expressed gene, and *KCNQ1* and *CDKN1C* are maternally expressed genes. The six CpG dinucleotides (CG1→CG6) examined by pyrosequencing are highlighted with a yellow rectangle, and the positions of PyF & PyR primers and SP are shown by thick arrows and a thin arrow, respectively. A pyrogram of case 3 is shown. (c) Array CGH analysis for chromosome 11p15.5 encompassing the ICR2 domain in case 3. A region encompassing KvDMR1 and *CDKN1C* is shown. Black, red and green dots denote signals indicative of the normal, the increased (>+0·5) and the decreased (<−1·0) copy numbers, respectively. Although several red and green signals are seen, there is no portion associated with ≥3 consecutive red or green signals.

Methylation analysis of KvDMR1 and array CGH analysis for chromosome 11p15.5

Increased expression of *CDKN1C*, as well as gain-of-function mutations of *CDKN1C*, may lead to IMAGe syndrome. Such increased *CDKN1C* expression would occur in association with hypermethylated KvDMR1 (differentially methylated region 1) at the ICR2 domain, because *CDKN1C* is expressed when the *cis*-situated KvDMR1 is methylated as observed after maternal transmission and is repressed when the *cis*-situated KvDMR1 is unmethylated as observed after paternal transmission.[5] Thus, we performed pyrosequencing analysis for six CpG dinucleotides (CG1–CG6) within KvDMR1, using bisulphite-treated leucocyte genomic DNA samples (Fig. 1b). In brief, a 155-bp region was PCR-amplified with a primer set (PyF and PyR) for both methylated and unmethylated clones, and a sequence primer (SP) was hybridized to single-stranded PCR products (for PyF, PyR and SP sequences, see Table S1). Subsequently, methylation index (MI, the ratio of methylated clones) was obtained for each CpG dinucleotide, using PyroMark Q24 (Qiagen, Hilden, Germany). To define the reference ranges of MIs, 50 control subjects were similarly studied with permission.

Increased *CDKN1C* expression may also result from a copy number gain of the maternally inherited ICR2 domain. Thus, we performed high-density array CGH (comparative genomic hybridization) using a custom-build 33 088 oligonucleotide probes for chromosome 11p15.5 encompassing the ICR2 domain, together with ~10 000 reference probes for other chromosomal regions (Agilent Technologies, Santa Clara, CA, USA). The procedure was carried out as described in the manufacturer's instructions.

Results

Clinical findings

Detailed clinical findings are shown in Table 1. Cases 1–3 exhibited characteristic faces with frontal bossing, flat nasal root, low set ears and mild micrognathia, as well as short limbs. They had IUGR and postnatal growth failure. Notably, while birth and present length/height and weight were severely compromised, birth and present occipitofrontal circumference (OFC) were relatively well preserved. Radiological examinations revealed generalized osteopenia, delayed bone maturation and metaphyseal dysplasia with vertical sclerotic striations of the knee in cases 1–3, slender bones in cases 1 and 2, scoliosis in cases 2 and 3, arachnodactyly in case 3 and broad distal phalanx of the thumbs and great toes in case 2 (Fig. 2). Cases 1 and 3 experienced adrenal crisis in early infancy and received glucocorticoid and mineralocorticoid supplementation therapy since infancy. Case 2 had transient neonatal hyponatremia and several episodes of hypoglycaemia without electrolyte abnormality in childhood and was found to have hypoglycaemia and hyponatremia without hyperkalemia when he had severe viral gastroenteritis at 15·5 years of age. Thus, an adrenocorticotropic hormone stimulation test was performed after recovery from gastroenteritis, revealing poor cortisol response. Thereafter, he was placed on glucocorticoid supplementation therapy. As serum electrolytes were normal, mineralocorticoid supplementation therapy was not initiated. Genital abnormalities included cryptorchidism and small testes in cases 2 and 3, and hypospadias in case 3. However, pituitary-gonadal endocrine function was apparently normal in cases 1–3. Urine calcium secretion was borderline high or increased in cases 1–3, although serum calcium and calcium homeostasis-related factors were normal. In addition, feeding difficulties during infancy were observed in cases 1 and 2, but not in case 3, and oligohydramnios was noticed during the pregnancy of case 2. There was no body asymmetry in cases 1–3. Thus, clinical studies in cases 1–3 revealed not only IMAGe syndrome-compatible phenotypes, but also hitherto undescribed clinical finding (Table 2).

Sequence analysis of CDKN1C

A heterozygous identical missense mutation (c.820G>A, p.Asp274Asn) was identified in cases 1 and 2 (Fig. 1a). This mutation occurred as a *de novo* event in case 1 and was inherited from the phenotypically normal mother in case 2. No demonstrable mutation was identified in case 3.

Methylation analysis of KvDMR1 and array CGH analysis for chromosome 11p15.5

The MIs for CG1–CG6 were invariably within the normal range in cases 1–3 (Fig. 1b), and no discernible copy number alteration was identified in cases 1–3 (Fig. 1c). The results excluded maternal uniparental disomy involving KvDMR1, hypermethylation (epimutation) of the paternally inherited KvDMR1 and submicroscopic duplication involving the maternally derived ICR2 domain, as well as submicroscopic deletion affecting the paternally derived ICR2 domain.

Discussion

CDKN1C mutations in IMAGe syndrome

We identified a heterozygous *CDKN1C* missense mutation (Asp274Asn) in cases 1 and 2. This mutation has previously been detected in a patient with IMAGe syndrome.[4] Furthermore, *de novo* occurrence of the mutation in case 1 argues for the mutation being pathologic, and maternal transmission of the mutation in case 2 is consistent with *CDKN1C* being a maternally expressed gene. Thus, our results provide further evidence for specific missense mutations of *CDKN1C* being responsible for the development of IMAGe syndrome.

Clinical features in CDKN1C*-mutation-positive cases 1 and 2*

Several matters are noteworthy with regard to clinical findings in *CDKN1C*-mutation-positive cases 1 and 2. First, although

Table 1. Clinical findings of cases 1–3

	Case 1*	Case 2	Case 3
Karyotype	46,XX	46,XY	46,XY
Present age (year)	8·5	16·5	15·0
Characteristic face	Yes	Yes	Yes
Pre- and postnatal growth			
Gestational age (week)	35	37	38
Birth length (cm) (SDS)	37·0 (−3·5)	40·0 (−4·0)	41·0 (−4·3)
Birth weight (kg) (SDS)	1·34 (−2·9)	2·03 (−3·5)	1·71 (−3·4)
Birth OFC (cm) (SDS)	30·7 (−0·3)	32·0 (−0·9)	33·0 (−0·1)
Birth BMI (kg/m^2) (percentile)	9·8 (<3)	12·7 (50)	10·1 (<3)
BMI (kg/m^2) at 2 years of age (SDS)	14·2 (−1·8)	13·0 (−3·4)	Unknown
Present height (cm) (SDS)	92·8 (−6·2)	124·7 (−7·8)	135·2 (−5·1)
Present weight (kg) (SDS)	16·0 (−1·9)	25·4 (−3·5)	30·4 (−2·6)
Present OFC (cm) (SDS)	52·0 (−0·2)	53·0 (−2·5)	Unknown
Present BMI (kg/m^2) (SDS)	18·6 (+1·6)	16·3 (−2·6)	16·6 (−1·7)
Skeletal abnormality			
Examined age (year)	5·5	16·5	15·0
Generalized osteopenia	Yes	Yes	Yes
Delayed maturation	Yes	Yes	Yes
Metaphyseal dysplasia	Yes	Yes	Yes
Slender bones	Yes	Yes	No
Scoliosis	No	Yes	Yes
Arachnodactyly	No	No	Yes
Broad thumbs & big toes	No	Yes	No
Adrenal dysfunction			
Examined age (year) before therapy	0·1 (39 days)	15·5	0·5 (6 months)
MRI/CT	Undetectable	Undetectable	Undetectable
ACTH (pg/ml)	9010 [19·9 ± 8·8]	427 [22·9 ± 6·2]	>1000 [22·9 ± 6·2]
Cortisol (μg/dl)	8·4 [8·3 ± 3·4]	6·9 [9·5 ± 2·9]	<1·0 [9·5 ± 2·9]
After ACTH stimulation†	N.E.	9·4 [> 20]	<1·0 [> 20]
Plasma renin activity (ng/ml/h)	N.E.	6·0 [1·0 ± 0·1]	>25 [1·01 ± 0·14]
Active renin concentration (pg/ml)	21 400 [2·5–21·4]	N.E.	N.E.
Aldosterone (ng/dl)	6·9 [9·7 ± 4·5]	5·2 [8·5 ± 1·4]	4·1 [7·4 ± 2·2]
Na (mEq/l)	122 [135–145]	141 (127‡) [135–145]	126 [135–145]
K (mEq/l)	8·0 [3·7–4·8]	4·2 (4·0‡) [3·7–4·8]	6·5 [3·7–4·8]
Cl (mEq/l)	86 [98–108]	103 (98‡) [98–108]	89 [98–108]
Glucocorticoid therapy	Yes (since 2 months)	Yes (since 15·5 years)	Yes (since 6 months)
Mineralocorticoid therapy	Yes (since 2 months)	No	Yes (since 6 months)
Genital abnormality			
Examined age (year)	8·5	16·5	15·0
Hypospadias	–	No	Yes (operated at 2 years)
Cryptorchidism	–	Yes (B) (operated at 2 years)	Yes (operated at 2 years)
Micropenis	–	No	No
Testis size (R & L) (ml)	–	5 & 8 [13–20]	4 & 10 [11–20]
Pubic hair (Tanner stage)	1 [10·0 ± 1·4 years]§	4 [14·9 ± 0·9 years]¶	4 [14·9 ± 0·9 years]¶
LH (mIU/ml)	<0·1 [<0·1–1·3]	3·9 [0·2–7·8]	4·8 [0·2–7·8]
After GnRH-stimulation**	3·5 [1·6–4·8]	N.E.	N.E.
FSH (mIU/ml)	0·7 [<0·1–5·4]	4·2 [0·3–18·4]	17·6 [0·3–18·4]
After GnRH-stimulation**	12·0 [10·7–38·1]	N.E.	N.E.
Testosterone (ng/ml)	–	4·3 [1·7–8·7]	3·7 [1·7–8·7]
Calcium metabolism			
Examined age (year)	8·5	16·5	15·0
Calcium (mg/dl)	9·7 [8·8–10·5]	9·2 [8·9–10·6]	9·8 [8·9–10·6]
Inorganic phosphate (mg/dl)	3·9 [3·7–5·6]	4·6 [3·1–5·0]	3·8 [3·2–5·1]
Alkaline phosphatase (IU/l)	458 [343–917]	623 [225–680]	309 [225–680]
Intact PTH (pg/ml)	23 [10–65]	43 [10–65]	28 [10–65]
PTHrP (pmol/l)	N.E.	<1·1 [<1·1]	N.E.

(continued)

Table 1. (continued)

	Case 1*	Case 2	Case 3
$1,25(OH)_2$ vitamin D (pg/ml)	50 [13–79]	67 [13–79]	50 [13–79]
Urine calcium/creatinine ratio (mg/mg)	0·82 [<0·25]	0·24 [<0·25]	0·44 [<0·25]
%TRP	92 [80–96]	95 [80–96]	94 [80–96]
Others	Feeding difficulties	Feeding difficulties Oligohydramnios	

SDS, standard deviation score; OFC, occipitofrontal circumference; BMI, body mass index; MRI, magnetic resonance imaging; CT, computed tomography; ACTH, adrenocorticotropic hormone; R, right; L, left; LH, luteinizing hormone; FSH, follicle-stimulating hormone; GnRH, gonadotropin-releasing hormone; PTH, parathyroid hormone; PTHrP, PTH-related protein; TRP, tubular reabsorption of phosphate; N.E., not examined; and B, bilateral.
Biochemical values indicate basal blood values, except for those specifically defined.
Birth and present length/height, weight, OFC and BMI have been assessed by sex- and gestational- or age-matched Japanese reference data reported in the literature[26,27] and in the Ministry of Health, Labor, and Welfare Database (http://www.e-stat.go.jp/SG1/estat/GL02020101.do).
The values in brackets represent age- and sex-matched reference values in Japanese children.[28]
The conversion factor to the SI unit: 0·220 for ACTH (pmol/l), 27·6 for cortisol (nmol/l), 0·028 for aldosterone (nmol/l), 3·46 for testosterone (nmol/l), 0·25 for calcium (nmol/l), 0·323 for inorganic phosphate (nmol/l), 0·106 for intact PTH (pmol/l), 2·40 for $1,25(OH)_2$ vitamin D (pmol/l) and 1·0 for plasma renin activity (μg/l/h), active renin concentration (ng/l), Na (nmol/l), K (nmol/l), Cl (nmol/l), LH (IU/l), FSH (IU/l), alkaline phosphatase (IU/l) and PTHrP (pmol/l).
*Clinical findings before 3 years of age have been reported previously.[7]
†ACTH 0·25 mg bolus i.v.; blood sampling at 60 min.
‡Electrolyte values at the time of severe gastroenteritis; other biochemical data in reference to adrenal dysfunction were obtained after recovery from gastroenteritis and before glucocorticoid supplementation therapy.
§Reference age for Tanner stage 2 breast development in Japanese girls.[29]
¶Reference age for Tanner stage 4 pubic hair development in Japanese boys.[29]
**GnRH 100 $\mu g/m^2$ bolus i.v.; blood sampling at 0, 30, 60, 90, and 120 min.

Table 2. Summary of clinical features of cases 1–3

	Case 1	Case 2	Case 3
CDKN1C mutation	Yes	Yes	No
Previously reported IMAGe syndrome-compatible phenotype			
IUGR	Yes	Yes	Yes
Metaphyseal dysplasia	Yes	Yes	Yes
Adrenal hypoplasia	Yes*	Yes*	Yes*
Genital abnormality	(Female)	Yes	Yes
Hypercalciura†	Yes	No	Yes
Hitherto undescribed findings			
Body habitus	Relative macrocephaly	Relative macrocephaly	Relative macrocephaly
Skeletal			Arachnodactyly Lack of slender bones
Adrenal		FGD-like phenotype with no obvious mineralocorticoid deficiency	
Genital	Apparently normal pituitary-gonadal endocrine function	Apparently normal pituitary-gonadal endocrine function	Apparently normal pituitary-gonadal endocrine function
Others	Feeding difficulties	Feeding difficulties Oligohydramnios	

IUGR, intrauterine growth retardation; and FGD, familial glucocorticoid deficiency.
*Undetectable on magnetic resonance imaging and/or computed tomography.
†Frequent but not invariable feature.

pre- and postnatal body growth was severely impaired, pre- and postnatal OFC was relatively well preserved. In this regard, while *CDKN1C* is preferentially expressed from the maternal allele in most tissues, it is biparentally expressed at least in the foetal brain.[10] This expression pattern would be relevant to the relative macrocephaly in IMAGe syndrome. Notably, the combination of severely compromised body growth and well-preserved OFC is also characteristic of Silver–Russell syndrome (SRS) resulting

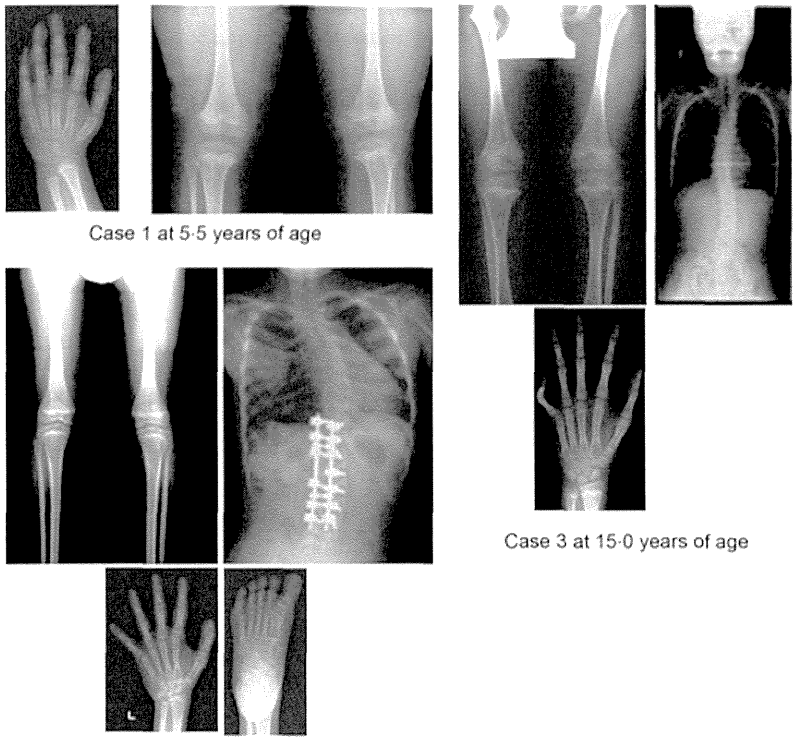

Fig. 2 Representative skeletal roentgenograms in cases 1–3.

from *H19*-DMR hypomethylation (epimutation),[11] and this is primarily consistent with paternal expression of the growth-promoting gene *IGF2* in the body and biparental expression of *IGF2* in the brain.[12] Thus, loss-of-imprinting in the brain tissue appears to underlie relative macrocephaly in both IMAGe syndrome and SRS.

Second, skeletal abnormalities including metaphyseal dysplasia were identified in cases 1 and 2. In this regard, skeletal phenotype of mice lacking *Cdkn1c* is grossly opposite of parathyroid hormone-related protein (PTHrP)-null phenotype,[13,14] and PTHrP permits skeletal development at least in part by suppressing *Cdkn1c* expression.[15] Thus, while serum calcium and calcium homeostasis-related factors were normal in cases 1 and 2, dysregulated PTHrP and/or PTH/PTHrP receptor signalling might be relevant to skeletal abnormalities in patients with gain-of-function mutations of *CDKN1C*. In addition, such a possible signalling defect might also be relevant to the frequent occurrence of hypercalciuria in IMAGe syndrome.

Third, adrenal dysfunction was mild in case 2, while case 1 experienced adrenal crisis in infancy as previously reported in patients with *CDKN1C* mutations.[1,3,4] Indeed, adrenal phenotype of case 2 is similar to that of patients with FGD rather than adrenal hypoplasia.[8,9] Our results therefore would expand the clinical spectrum of adrenal dysfunction in patients with *CDKN1C* mutations. For adrenal dysfunction, cortisol and aldosterone values remained within the normal range at the time of adrenal crisis in case 1 (Table 1). However, as adrenocorticotropic hormone and active renin concentrations were markedly increased, the overall results would be consistent with primary hypoadrenalism, as has been described previously.[16] This notion would also apply to the adrenal dysfunction in case 3 who had apparently normal aldosterone value and markedly increased plasma renin activity at the time of adrenal crisis.

Lastly, although male case 2 had bilateral cryptorchidism and small testes, pituitary-gonadal endocrine function was apparently normal as was secondary sexual development. Previously reported patients with *CDKN1C* mutations, as well as those who have not been examined for *CDKN1C* mutations, also have undermasculinized external genitalia in the presence of apparently normal endocrine function and pubertal development.[1–4,17,18] Notably, an episode of oligohydramnios was found in case 2 and has also been described in a 46,XY IMAGe syndrome patient with cryptorchidism.[19] This may imply the presence of placental hypoplasia and resultant chorionic gonadotropin deficiency as an underlying factor for genital anomalies.[11] In support of this notion, imprinted genes are known to play a pivotal role in body and placental growth,[20] and SRS is often associated with oligohydramnios, placental hypoplasia and undermasculinization.[11,21]

Genetic heterogeneity in IMAGe syndrome

Molecular data in case 3 imply the presence of genetic heterogeneity in IMAGe syndrome. Indeed, there was neither demonstrable *CDKN1C* mutation nor evidence for increased *CDKN1C* expression, while a pathologic mutation leading to gain-of-function or

increased expression of *CDKN1C* might reside on an unexamined region(s) such as promoter or enhancer sequences. In this regard, while case 3 showed IMAGe syndrome-compatible clinical features such as IUGR, metaphyseal dysplasia, adrenal hypoplasia and genital abnormalities, case 3 lacked slender bones and had arachnodactyly, in contrast to *CDKN1C*-mutation-positive cases 1 and 2. Such mild but discernible phenotypic variation might reflect the genetic heterogeneity. This matter might be clarified in the future by extensive studies such as exome or whole-genome sequencing. In particular, when such *CDKN1C*-mutation-negative patients with IMAGe syndrome-compatible phenotype have been accumulated, a novel gene(s) mutated in such patients may be identified. In this regard, if such a gene(s) exist, it is predicted to reside in the signal transduction pathway involving *CDKN1C*.

Relevance of CDKN1C mutations to atypical IMAGe syndrome and SRS

CDKN1C mutations have also been identified in atypical IMAGe syndrome and SRS (Fig. 1a). Hamajima *et al.* revealed a maternally inherited p.Ile272Ser mutation in three siblings (two males and one female) who manifested IUGR and adrenal insufficiency, and male genital abnormalities, but had no skeletal lesion.[22] Similarly, Brioude *et al.* found a maternally transmitted p.Arg279Leu mutation in six relatives (all females) from a four-generation family who satisfied the SRS diagnostic criteria,[23,24] after studying 97 SRS patients without known causes of SRS, that is, hypomethylation (epimutation) of the *H19*-DMR, duplication of the ICR2 and maternal uniparental disomy for chromosome 7 (upd(7)mat).[24] Notably, although both mutations had no significant effect on a cell cycle, they were associated with increased protein stability that appears to be consistent with the gain-of-function effects.[22,24] Such increased stability was also found for IMAGe-associated missense mutant proteins,[22] and an altered cell cycle with a significantly higher proportion of cells in the G1 phase was shown for an IMAGe-associated p.Arg279Pro mutation.[24] It is possible therefore that relatively severe *CDKN1C* gain-of-function effects lead to IMAGe syndrome and relatively mild *CDKN1C* gain-of-function effects result in SRS, with intermediate *CDKN1C* gain-of-function effects being associated with atypical IMAGe syndrome.[24]

Thus, it would not be surprising that cases 1–3 also met the SRS diagnostic criteria (Table 3).[23,24] Indeed, cases 1–3, as well as *CDKN1C*-mutation-positive SRS patients,[24] exhibited pre- and post-natal growth failure with relative macrocephaly and frequently manifested feeding difficulties and/or low body mass index (BMI) at two years of age. However, while relative macrocephaly is usually obvious at birth in SRS patients with *H19*-DMR epimutations and upd(7)mat,[21,23,25] it is more obvious at 2 years of age than at birth in *CDKN1C*-mutation-positive SRS patients.[24] Furthermore, *CDKN1C*-mutation-positive SRS patients are free from body asymmetry,[24] as are typical and atypical IMAGe syndrome patients described in this study and in the previous studies.[1–4,7,22] Thus, SRS caused by *CDKN1C* mutations may be characterized by clinically discernible macrocephaly at two years of age and lack of body asymmetry.

Table 3. Silver–Russell syndrome phenotypes in cases 1–3 and in affected relatives reported by Brioude *et al.*

	Case 1	Case 2	Case 3	Brioude *et al.**
Mandatory criteria				
IUGR†	Yes	Yes	Yes	4/4
Scoring system criteria				
Postnatal short stature (≤−2 SDS)	Yes	Yes	Yes	4/4
Relative macrocephaly‡	Yes	Yes	Yes	4/4§
Prominent forehead during early childhood	Yes	Yes	Yes	4/4
Body asymmetry	No	No	No	0/4
Feeding difficulties during early childhood and/or low BMI (<−2·0 SDS) around 2 years of age	Yes	Yes	Unknown	3/4 (1/4 & 2/4)¶

IUGR, Intrauterine growth retardation; SDS, standard deviation score; and BMI, body mass index.
The SRS diagnostic criteria proposed by Netchine *et al.*[23] and Brioude *et al.*[24] (low BMI around 2 years of age is included in Brioude *et al.*, but not in Netchine *et al.*): The diagnosis of SRS is made, when mandatory criteria plus at least three of the five scoring system criteria are observed. For detailed clinical features in cases 1–3, see Table 1.
*While six relatives were found to have *CDKN1C* mutation, detailed clinical features have been obtained in four mutation-positive relatives.[24]
†Birth length and/or birth weight ≤−2 SDS for gestational age.
‡SDS for birth length or birth weight minus SDS for birth occipitofrontal circumference ≤−1·5.
§Relative macrocephaly is more obvious at 2 years of age (4/4) than at birth (2/4).
¶One patient is positive for feeding difficulties, and other two patients are positive for low BMI.

Conclusion

In summary, we studied three patients with IMAGe syndrome. The results provide implications for phenotypic spectrum, underlying factor(s) in the development of each phenotype and genetic heterogeneity in IMAGe syndrome, as well as a phenotypic overlap between IMAGe syndrome and SRS. Further studies will permit to elucidate such matters.

Funding

This study was supported in part by Grants-in-Aid for Scientific Research (A) (25253023) and for Scientific Research on Innovative Areas (22132004-A01) from the Ministry of Education, Culture, Sports, Science and Technology, by Grant for Research on Intractable Diseases from the Ministry of Health, Labor and Welfare (H24-048), and by Grants from National Center for Child Health and Development (23A-1, 24-7 and 25-10).

Declaration of interest

The authors have nothing to declare.

References

1 Vilain, E., Le Merrer, M., Lecointre, C. *et al.* (1999) IMAGe, a new clinical association of intrauterine growth retardation, metaphyseal dysplasia, adrenal hypoplasia congenita, and genital anomalies. *Journal of Clinical Endocrinology and Metabolism*, **84**, 4335–4340.

2 Balasubramanian, M., Sprigg, A. & Johnson, D.S. (2010) IMAGe syndrome: case report with a previously unreported feature and review of published literature. *American Journal of Medical Genetics A*, **152A**, 3138–3142.

3 Bergadá, I., Del Rey, G., Lapunzina, P. *et al.* (2005) Familial occurrence of the IMAGe association: additional clinical variants and a proposed mode of inheritance. *Journal of Clinical Endocrinology and Metabolism*, **90**, 3186–3190.

4 Arboleda, V.A., Lee, H., Parnaik, R. *et al.* (2012) Mutations in the PCNA-binding domain of CDKN1C cause IMAGe syndrome. *Nature Genetics*, **44**, 788–792.

5 Demars, J. & Gicquel, C. (2012) Epigenetic and genetic disturbance of the imprinted 11p15 region in Beckwith-Wiedemann and Silver-Russell syndromes. *Clinical Genetics*, **81**, 350–361.

6 Lee, M.-H., Reynisdottir, I. & Massague, J. (1995) Cloning of p57(KIP2), a cyclin-dependent kinase inhibitor with unique domain structure and tissue distribution. *Genes and Development*, **9**, 639–649.

7 Amano, N., Naoaki, H., Ishii, T. *et al.* (2008) Radiological evolution in IMAGe association: a case report. *American Journal of Medical Genetics A*, **146A**, 2130–2133.

8 El-Khairi, R., Martinez-Aguayo, A., Ferraz-de-Souza, B. *et al.* (2011) Role of DAX-1 (NR0B1) and steroidogenic factor-1 (NR5A1) in human adrenal function. *Endocrine Development*, **20**, 38–46.

9 Meimaridou, E., Hughes, C.R., Kowalczyk, J. *et al.* (2013) Familial glucocorticoid deficiency: new genes and mechanisms. *Molecular and Cellular Endocrinology*, **371**, 195–200.

10 Matsuoka, S., Thompson, J.S., Edwards, M.C. *et al.* (1996) Imprinting of the gene encoding a human cyclin-dependent kinase inhibitor, p57KIP2, on chromosome 11p15. *Proceedings of the National Academy of Sciences of the USA*, **93**, 3026–3030.

11 Yamazawa, K., Kagami, M., Nagai, T. *et al.* (2008) Molecular and clinical findings and their correlations in Silver-Russell syndrome: implications for a positive role of IGF2 in growth determination and differential imprinting regulation of the IGF2-H19 domain in bodies and placentas. *Journal of Molecular Medicine*, **86**, 1171–1181.

12 Ulaner, G.A., Yang, Y., Hu, J.F. *et al.* (2003) CTCF binding at the insulin-like growth factor-II (IGF2)/H19 imprinting control region is insufficient to regulate IGF2/H19 expression in human tissues. *Endocrinology*, **144**, 4420–4426.

13 Zhang, P., Leigeois, N.J., Wong, C. *et al.* (1997) Altered cell differentiation and proliferation in mice lacking p57(KIP2) indicates a role in Beckwith-Wiedemann syndrome. *Nature*, **387**, 151–158.

14 Karaplis, A.C., Luz, A., Glowacki, J. *et al.* (1994) Lethal skeletal dysplasia from targeted disruption of the parathyroid hormone-related peptide gene. *Genes & Development*, **8**, 277–289.

15 MacLean, H.E., Guo, J., Knight, M.C. *et al.* (2004) The cyclin-dependent kinase inhibitor p57(Kip2) mediates proliferative actions of PTHrP in chondrocytes. *Journal of Clinical Investigation*, **113**, 1334–1343.

16 Stewart, P.M. & Krone, N.P. (2011) The adrenal cortex. In: S. Melmed, K.S. Polonsky, P.R. Larsen, H.N. Kronenberg eds. Williams Textbook of Endocrinology, 12th edn. Elsevier, Saunders, 479–577.

17 Lienhardt, A., Mas, J.C., Kalifa, G. *et al.* (2002) IMAGe association: additional clinical features and evidence for recessive autosomal inheritance. *Hormone Research*, **57**(Suppl 2), 71–78.

18 Pedreira, C.C., Savarirayan, R. & Zacharin, M.R. (2004) IMAGe syndrome: a complex disorder affecting growth, adrenal and gonadal function, and skeletal development. *Journal of Pediatrics*, **144**, 274–277.

19 Ko, J.M., Lee, J.H., Kim, G.H. *et al.* (2007) A case of a Korean newborn with IMAGe association presenting with hyperpigmented skin at birth. *European Journal of Pediatrics*, **166**, 879–880.

20 Fowden, A.L., Sibley, C., Reik, W. *et al.* (2006) Imprinted genes, placental development and fetal growth. *Hormone Research*, **65** (Suppl 3), 50–58.

21 Wakeling, E.L., Amero, S.A., Alders, M. *et al.* (2010) Epigenotype-phenotype correlations in Silver-Russell syndrome. *Journal of Medical Genetics*, **47**, 760–768.

22 Hamajima, N., Johmura, Y., Suzuki, S. *et al.* (2013) Increased protein stability of CDKN1C causes a gain-of-function phenotype in patients with IMAGe syndrome. *PLoS ONE*, **8**, e75137.

23 Netchine, I., Rossignol, S., Dufourg, M.N. *et al.* (2007) 11p15 imprinting center region 1 loss of methylation is a common and specific cause of typical Russell-Silver syndrome: clinical scoring system and epigenetic-phenotypic correlations. *Journal of Clinical Endocrinology and Metabolism*, **92**, 3148–3154.

24 Brioude, F., Oliver-Petit, I., Blaise, A. *et al.* (2013) CDKN1C mutation affecting the PCNA-binding domain as a cause of familial Russell Silver syndrome. *Journal of Medical Genetics*, **50**, 823–830.

25 Fuke, T., Mizuno, S., Nagai, T. *et al.* (2013) Molecular and clinical studies in 138 Japanese patients with Silver-Russell syndrome. *PLoS ONE*, **8**, e60105.

26 Suwa, S., Tachibana, K., Maesaka, H. *et al.* (1992) Longitudinal standards for height and height velocity for Japanese children from birth to maturity. *Clinical Pediatric Endocrinology*, **1**, 5–14.

27 Inokuchi, M., Matsuo, N., Anzo, M. *et al.* (2007) Body mass index reference values (mean and SD) for Japanese children. *Acta Paediatrica*, **96**, 1674–1676.

28 Japan Public Health Association. (1996) Normal Biochemical Values in Japanese Children. Sanko Press, Tokyo, (in Japanese).

29 Matsuo, N. (1993) Skeletal and sexual maturation in Japanese children. *Clinical Pediatric Endocrinology*, **2**(Suppl), 1–4.

Supporting Information

Additional Supporting Information may be found in the online version of this article:

Table S1. Primers utilized in this study.

ORIGINAL RESEARCH ARTICLE | Genetics inMedicine

Open

Comprehensive and quantitative multilocus methylation analysis reveals the susceptibility of specific imprinted differentially methylated regions to aberrant methylation in Beckwith–Wiedemann syndrome with epimutations

Toshiyuki Maeda, MD[1,2], Ken Higashimoto, PhD[1], Kosuke Jozaki, PhD[1], Hitomi Yatsuki, PhD[1], Kazuhiko Nakabayashi, PhD[3], Yoshio Makita, PhD[4], Hidefumi Tonoki, PhD[5], Nobuhiko Okamoto, MD[6], Fumio Takada, PhD[7], Hirofumi Ohashi, PhD[8], Makoto Migita, PhD[9], Rika Kosaki, MD[10], Keiko Matsubara, PhD[11], Tsutomu Ogata, PhD[12], Muneaki Matsuo, PhD[2], Yuhei Hamasaki, PhD[2], Yasufumi Ohtsuka, MD[1,2], Kenichi Nishioka, PhD[1], Keiichiro Joh, PhD[1], Tsunehiro Mukai, PhD[13], Kenichiro Hata, PhD[3] and Hidenobu Soejima, PhD[1]

Purpose: Expression of imprinted genes is regulated by DNA methylation of differentially methylated regions (DMRs). Beckwith–Wiedemann syndrome is an imprinting disorder caused by epimutations of DMRs at 11p15.5. To date, multiple methylation defects have been reported in Beckwith–Wiedemann syndrome patients with epimutations; however, limited numbers of DMRs have been analyzed. The susceptibility of DMRs to aberrant methylation, alteration of gene expression due to aberrant methylation, and causative factors for multiple methylation defects remain undetermined.

Methods: Comprehensive methylation analysis with two quantitative methods, matrix-assisted laser desorption/ionization mass spectrometry and bisulfite pyrosequencing, was conducted across 29 DMRs in 54 Beckwith–Wiedemann syndrome patients with epimutations. Allelic expressions of three genes with aberrant methylation were analyzed. All DMRs with aberrant methylation were sequenced.

Results: Thirty-four percent of *Kv*DMR1–loss of methylation patients and 30% of *H19*DMR–gain of methylation patients showed multiple methylation defects. Maternally methylated DMRs were susceptible to aberrant hypomethylation in *Kv*DMR1–loss of methylation patients. Biallelic expression of the genes was associated with aberrant methylation. *Cis*-acting pathological variations were not found in any aberrantly methylated DMR.

Conclusion: Maternally methylated DMRs may be vulnerable to DNA demethylation during the preimplantation stage, when hypomethylation of *Kv*DMR1 occurs, and aberrant methylation of DMRs affects imprinted gene expression. *Cis*-acting variations of the DMRs are not involved in the multiple methylation defects.

Genet Med advance online publication 8 May 2014

Key Words: Beckwith–Wiedemann syndrome; DNA methylation; differentially methylated region; genomic imprinting; multiple methylation defects

INTRODUCTION

Genomic imprinting is an epigenetic phenomenon that leads to parent-specific differential expression of a subset of mammalian genes. Most imprinted genes are clustered in regions called imprinting domains, and the expression of imprinted genes within these domains is regulated by imprinting control regions.[1,2] Differentially methylated regions (DMRs), which are defined as having DNA methylation on only one of the two parental alleles, play critical roles in the regulation of imprinting. There are two kinds of DMRs: maternally methylated DMRs (matDMRs) and paternally methylated DMRs (patDMRs). In addition, there is another classification, gametic DMRs and somatic DMRs, based on the timing of the establishment of differential methylation. Gametic DMRs acquire DNA methylation during gametogenesis, and the methylation is maintained from zygote to somatic cells during all developmental stages. Most gametic DMRs are identical to imprinting control regions. On the other hand, somatic DMRs are established during early embryogenesis after fertilization under the control of nearby imprinting control regions.[1,2] Because imprinted genes play an important role in the growth and development of embryos, placental formation, and metabolism, aberrant expression of

[1]Division of Molecular Genetics and Epigenetics, Department of Biomolecular Sciences, Faculty of Medicine, Saga University, Saga, Japan; [2]Department of Pediatrics, Faculty of Medicine, Saga University, Saga, Japan; [3]Department of Maternal–Fetal Biology, National Research Institute for Child Health and Development, Tokyo, Japan; [4]Education Center, Asahikawa Medical University, Asahikawa, Japan; [5]Department of Pediatrics, Maternal, Perinatal, and Child Medical Center, Tenshi Hospital, Sapporo, Japan; [6]Department of Medical Genetics, Osaka Medical Center and Research Institute for Maternal and Child Health, Izumi, Japan; [7]Department of Medical Genetics, Kitasato University Graduate School of Medical Sciences, Kanagawa, Japan; [8]Division of Medical Genetics, Saitama Children's Medical Center, Saitama, Japan; [9]Department of Pediatrics, Nippon Medical School, Tokyo, Japan; [10]Division of Medical Genetics, National Center for Child Health and Development, Tokyo, Japan; [11]Department of Molecular Endocrinology, National Research Institute for Child Health and Development, Tokyo, Japan; [12]Department of Pediatrics, Hamamatsu University School of Medicine, Hamamatsu, Japan; [13]Nishikyushu University, Saga, Japan. Correspondence: Hidenobu Soejima (soejimah@cc.saga-u.ac.jp)

Submitted 10 November 2013; accepted 7 April 2014; advance online publication 8 May 2014. doi:10.1038/gim.2014.46

imprinted genes due to epigenetic or genetic abnormalities is implicated in the pathogenesis of some human disorders, such as congenital anomalies and tumors.[1,2]

Beckwith–Wiedemann syndrome (BWS; Online Mendelian Inheritance in Man (OMIM) #130650) is an imprinting disease that is characterized by prenatal and postnatal macrosomia, macroglossia, abdominal wall defects, and variable minor features. The relevant imprinted chromosomal region in BWS is 11p15.5, which consists of two imprinted domains, *IGF2/H19* and *CDKN1C/KCNQ1OT1*, *H19*DMR and *Kv*DMR1 being the respective imprinting control regions.[3–5] Among several causative alterations identified so far, loss of methylation (LOM) at *Kv*DMR1 and gain of methylation (GOM) at *H19*DMR are isolated epimutations. Hypomethylation at multiple imprinted DMRs has been reported in patients with transient neonatal diabetes mellitus type 1,[6] and the same phenomenon, referred to as multiple methylation defects (MMDs), has been reported in BWS patients with *Kv*DMR1-LOM.[7–13] However, although the human genome contains more than 30 imprinting domains (http://www.geneimprint.com), a limited number of imprinted DMRs have been analyzed so far, with the exception of a report by Court et al.[12] In addition, methods used for methylation analysis have ranged from nonquantitative to quantitative approaches, and although some studies have used only one method for methylation analysis,[8,9,11] others have used two or more in conjuction.[7,10–13] Furthermore, the questions of whether susceptibility to aberrant methylation is different in each type of DMR, whether aberrant methylation indeed affects imprinted gene expression, and what causative factors are responsible for MMDs still remain unanswered. To clarify these issues, we have conducted a comprehensive methylation screening in BWS patients with *Kv*DMR1-LOM or *H19*DMR-GOM with a quantitative method, matrix-assisted laser desorption/ionization mass spectrometry (MALDI-TOF MS), on 29 imprinted DMRs, which represents the largest number of DMRs analyzed to date, followed by confirmation with another quantitative method, bisulfite pyrosequencing. We also performed gene expression analysis and sequencing of aberrantly methylated DMRs. We found that matDMRs are susceptible to aberrant methylation. We also found alterations in imprinted gene expression due to the aberrant methylation and no *cis*-acting pathological variations in DMRs with MMDs.

MATERIALS AND METHODS

Patients

Fifty-four BWS patients (25 boys, 26 girls, 3 gender-unspecified patients; average age: 3.0 years (0–13.9 years)) and their parents were enrolled in this study. Among them, 46 patients met clinical criteria for BWS as described by Weksberg et al.[3] and 6 patients met clinical criteria as described by DeBaun et al.[14] (**Supplementary Table S1** online). Because two patients were clinically diagnosed more than 20 years ago, their specific diagnostic criteria were unknown. The methylation statuses of *H19*DMR and *Kv*DMR1, paternal uniparental disomy of chromosome 11 (upd(11)pat), and *CDKN1C* mutations were screened as described previously.[15–17] Peripheral blood samples of most patients were subjected to standard G-banding chromosome analysis and/or high-resolution G-band patterning of human chromosome 11, but neither assay showed any abnormalities in any patient (data not shown). Among the 54 patients, 44 displayed *Kv*DMR1-LOM but did not show other causative alterations, including *H19*DMR-GOM, upd(11)pat, and *CDKN1C* mutations (data not shown). The remaining 10 patients displayed *H19*DMR-GOM but did not show other causative alterations (data not shown). We sequenced the entire *H19*DMR in *H19*DMR-GOM patients and found no mutations.[18] We used the peripheral blood samples of 24 children (11 boys, 13 girls; average age: 3.8 years (range of 0–8 years)) who visited the Department of Pediatrics, Saga University Hospital, as normal controls having only mild illness such as common cold. This study was approved by the Ethics Committee for Human Genome and Gene Analyses of the Faculty of Medicine, Saga University. Written informed consent was obtained from the parents or the guardians of the patients and participants.

DNA isolation and bisulfite conversion

Genomic DNA was extracted from the peripheral blood of patients using the FlexiGene DNA Kit (Qiagen, Hilden, Germany) according to the manufacturer's instructions. A total of 1 μg of genomic DNA was subjected to bisulfite conversion using the EZ DNA Methylation Kit (Zymo Research, Irvine, CA), and then the converted DNA was eluted in 100 μl of water. Unmethylated control DNA was created by whole-genome amplification using the REPLI-g Mini Kit (Qiagen). To prepare fully methylated control DNA, the unmethylated DNA created by whole-genome amplification was treated twice with *Sss*I methylase.

Methylation analysis by MALDI-TOF MS

The DNA methylation status of imprinted DMRs was analyzed by MALDI-TOF MS analysis with a MassARRAY system (Sequenom, San Diego, CA) as previously described.[19,20] Briefly, each DMR was amplified by bisulfite-mediated polymerase chain reaction (PCR) using a primer set containing a primer carrying the T7 promoter sequence at the 5′ end. In vitro transcription of the PCR product was performed with T7 RNA polymerase, and the transcript was subjected to uracil-specific cleavage with RNase A. MALDI-TOF MS analysis of the cleaved fragments produced signal pattern pairs indicative of nonmethylated and methylated DNA. Epityper software (Sequenom) analysis of the signals yielded a methylation index (MI) ranging from 0 (no methylation) to 1 (full methylation) for each CpG unit, which contained one or more CpG sites. Aberrant methylation of a CpG unit was defined as the condition in which the difference of MIs between each patient and the average of normal controls exceeded 0.15. This definition was based on our finding in methylation-sensitive Southern blots, which revealed that the differences in MI for *Kv*DMR1-LOM or *H19*DMR-GOM in BWS patients were ≥0.15 (data not shown). Because the analyzed DMRs included several CpG units, aberrant methylation of each DMR was defined as the situation in which more

than 60% of the total number of analyzed CpG units showed aberrant methylation (with the MI difference exceeding 0.15). In the case of *IGF2*-DMR0, the three CpG sites were analyzed based on previous reports.[21,22] All primers used in this study are shown in **Supplementary Table S2** online.

Methylation analysis by bisulfite pyrosequencing

The aberrant methylation status of DMRs identified by MALDI-TOF MS was confirmed by bisulfite pyrosequencing using QIAGEN PyroMark Q24 according to the manufacturer's instructions (Qiagen). Primers for bisulfite-mediated PCR and pyrosequencing were designed using PyroMark Assay Design 2.0 (Qiagen). In analogy with MALDI-TOF MS analysis, aberrant methylation of a CpG site was defined as the situation in which the difference of MIs between each patient and the average of normal controls exceeded 0.15. Aberrant methylation of each DMR was defined as the condition in which more than 60% of the total number of analyzed CpG sites showed aberrant methylation (with the MI difference exceeding 0.15).

Bisulfite sequencing

Bisulfite sequencing was performed to analyze allelic methylation of *ZDBF2*-DMR. After PCR amplification, the PCR products were cloned into a pT7Blue T-Vector (Novagen, Darmstadt, Germany), and individual clones were sequenced. Parental alleles were distinguished by a single-nucleotide polymorphism (SNP, *rs1861437*) within the DMR.

Expression analysis of *ZDBF2*, *FAM50B*, and *GNAS1A*

Total RNA was extracted from the peripheral blood of patients using the QIAamp RNA Blood Mini Kit (Qiagen). The RNA was treated with RNase-free DNase I, and reverse transcription was performed with random primers. We used SNPs for allelic expression to distinguish between the two parental alleles: *rs10932150* in exon 5 of *ZDBF2*; *rs6597007* in exon 2 of *FAM50B*; and *rs143800311*, which is a 5-bp deletion/insertion variation in exon 1A of *GNAS1A*. Reverse transcription–PCR (RT-PCR) products encompassing the SNPs of *ZDBF2* and *FAM50B* were directly sequenced. The products encompassing the deletion/insertion variation of *GNAS1A* were separated by electrophoresis on an Applied Biosystems 3130 genetic analyzer (Applied Biosystems, Foster City, CA) and then analyzed with GeneMapper software (Applied Biosystems). Total expression levels of *ZDBF2* and *FAM50B* were quantitated by real-time PCR with TaqMan probes (Applied Biosystems). The expression level of each gene was normalized against that of the housekeeping genes encoding hydroxymethylbilane synthase (*HMBS*) and glyceraldehyde-3-phosphate dehydrogenase (*GAPDH*). All quantitative RT-PCRs were performed in triplicate.

Sequencing of aberrantly methylated DMRs

Direct sequencing of all DMRs showing aberrant methylation in *Kv*DMR1-LOM patients was performed to determine whether there was any pathological variation.

Statistical analyses

Fisher's exact test was used for the comparison of aberrant methylated DMRs. Fisher's exact test or Mann–Whitney *U*-test was used for statistical analyses of clinical features between MMDs and monolocus methylation defects in *Kv*DMR1-LOM patients. A P value < 0.05 was considered statistically significant.

RESULTS

Validation of methylation analyses, MALDI-TOF MS, and bisulfite pyrosequencing

First, we selected 37 regions reported previously as imprinted DMRs in the human genome[16,20,23] (refer to http://www.geneimprint.com/). To validate the quantitative capability of MALDI-TOF MS methylation analysis, mixtures of the unmethylated control DNA and the fully methylated control DNA (0, 25, 50, 75, and 100% methylated DNA) were subjected to bisulfite conversion and analyzed. We found a significant correlation between the measured MIs and predicted MIs in all DMRs, except for *GRB10*, *PEG13*, and IG-DMR-CG4 (**Supplementary Figure S1** online). Furthermore, in normal leukocytes, two regions (*TCEB3C*, *USP29*) showed mostly full methylation and three regions (*TP73*, *SPTBN1*, *WT1-AS*) showed mostly no methylation, suggesting that these regions were not differentially methylated in leukocytes (data not shown). Therefore, we excluded these eight regions and decided to analyze the remaining 29 DMRs by MALDI-TOF MS. Second, we obtained MIs from 24 normal controls using MALDI-TOF MS and calculated the average and SD of each CpG unit. We excluded CpG units in which SDs were >0.1 from further analysis. Averages and SDs of all CpG units analyzed in this study are shown in **Supplementary Table S3** online. After the MALDI-TOF MS analysis, we used bisulfite pyrosequencing to confirm the aberrant methylation uncovered. We also obtained MIs from the 24 controls using bisulfite pyrosequencing and calculated the average and SD of each CpG site. We excluded one CpG site in *H19*DMR because its SD was >0.1 due to a known SNP (*rs10732516*). Averages and SDs of control CpG sites are shown in **Supplementary Table S3** online. Finally, we compared the MIs of MALDI-TOF MS and bisulfite pyrosequencing of each DMR and found a significant correlation (**Supplementary Figure S2** online).

Multilocus methylation defects in BWS patients with epimutations

Among the 44 *Kv*DMR1-LOM patients, 15 (34.1%) showed aberrantly methylated DMRs outside of *Kv*DMR1: six showed aberrant methylation at only one DMR, and the other nine showed two or more methylated DMRs (**Figure 1a** and **Supplementary Figure S3** online). The greatest number of aberrantly methylated DMRs was found in patient BWS-s113, who exhibited 12 DMRs. Most of the aberrantly methylated DMRs demonstrated LOM, which was seen at *ARHI*-CG1, *ARHI*-CG2, *ARHI*-CG3, *FAM50B*, *ZAC*, *IGF2R*-DMR2, *MEST*, *NNAT*, *L3MBTL1*, *NESPAS*, *GNASXL*, and *GNAS1A*. Among them, the most frequently hypomethylated DMRs were

ARHI-CG1 and *ARHI*-CG3, found in nine (20.5%) and eight (18.2%) patients, respectively. By contrast, three DMRs, located at *ZDBF2*, *NESP*, and *MCTS2*, showed GOM, which was found in six (13.6%), two (4.5%), and one (2.3%) patients, respectively. *GNASXL*-DMR showed GOM in one patient (2.3%), whereas four patients (9.1%) showed LOM. The other 13 DMRs were not aberrantly methylated in any *Kv*DMR1-LOM patient.

Among the 10 *H19*DMR-GOM patients, all patients showed GOM at the *H19* promoter DMR, which was usually observed with loss of imprinting of *IGF2* (**Figure 1b**).[24] Four patients showed GOM at either *IGF2*-DMR0 or *IGF2*-DMR2; two patients showed GOM at both. Moreover, both LOM and GOM at other DMRs were found: LOM was found at *INPP5Fv2*-DMR in patients BWS-s015 and BWS-s064, and GOM was found at *NESP*-DMR in patient BWS-s012.

In addition, to exclude aberrantly methylated DMRs resulting from chromosome abnormalities such as uniparental disomy and copy number abnormality, microsatellite analyses using patients' and their parents' DNA were performed on all DMRs showing aberrant methylation. For quantitative analyses, tetranucleotide repeat markers near the imprinted DMRs were used (**Supplementary Materials and Methods** online). We found that no DMRs, except for six DMRs in three patients, exhibited any chromosome abnormalities (summarized in **Supplementary Figure S4** online). These results strongly suggest that the aberrant methylation of DMRs observed was

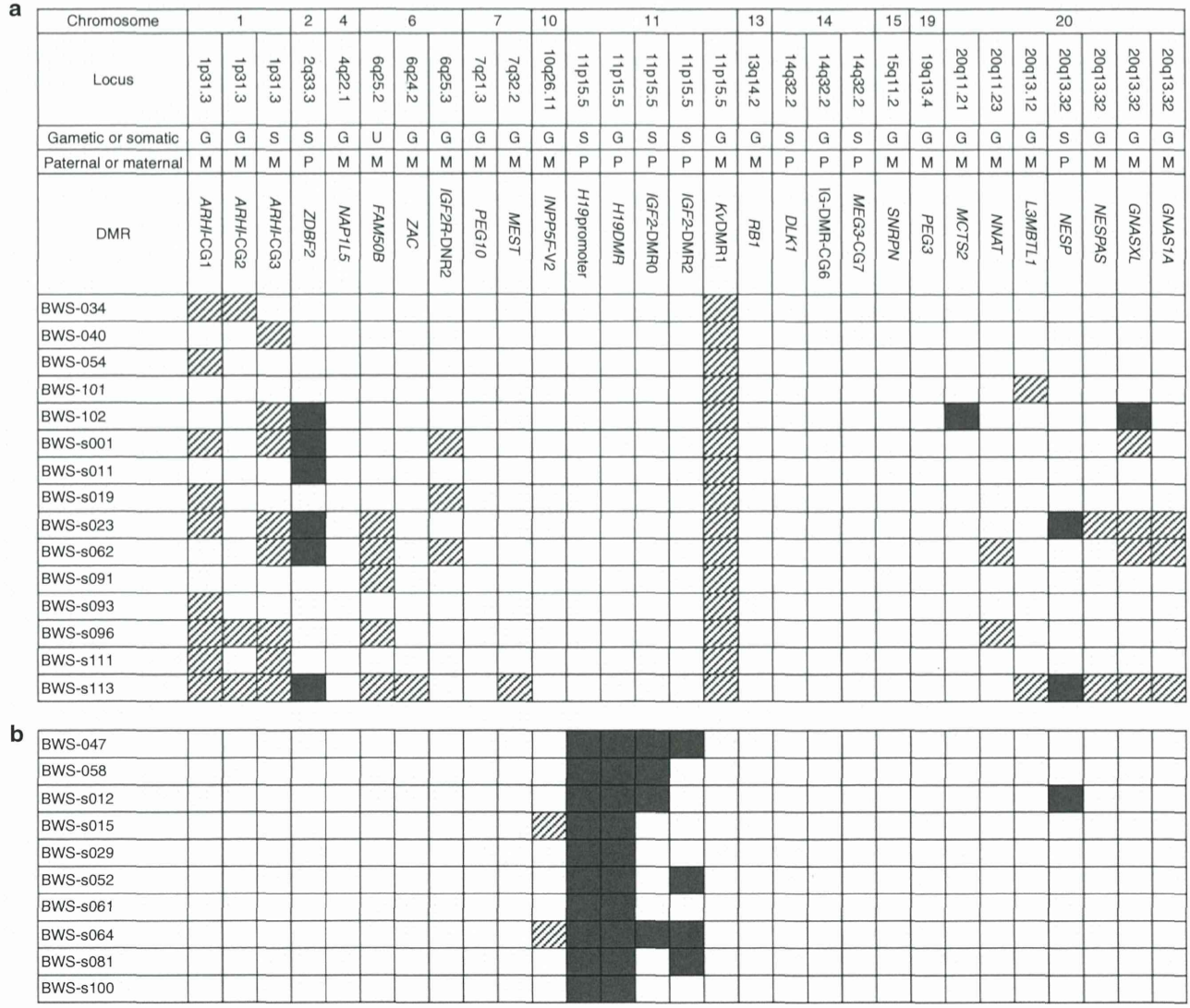

Figure 1 Results of methylation analyses of 29 imprinted differentially methylated regions (DMRs) in Beckwith–Wiedemann syndrome patients with epimutations. (**a**) Results of patients with *Kv*DMR1-LOM. Only the results of multiple methylation defects are shown. Aberrant methylation was confirmed by two quantitative methods: matrix-assisted laser desorption/ionization mass spectrometry and bisulfite pyrosequencing. The definition of aberrant methylation used here is described in the Materials and Methods section. Shaded rectangle: aberrant hypomethylation; dark gray rectangle: aberrant hypermethylation. (**b**) Results of all patients with *H19*DMR-GOM. GOM, gain of methylation; LOM, loss of methylation.

an isolated epimutation and was not due to chromosome abnormalities.

Comparison of aberrantly methylated DMRs

We found that 34.1% (15 of 44) of *Kv*DMR1-LOM patients and 30.0% (3 of 10) of *H19*DMR-GOM patients showed MMDs (**Figure 1a**). There was no statistical difference between them ($P > 0.99$, Fisher's exact test).

Among the 29 DMRs analyzed, there were 20 gametic DMRs and 8 somatic DMRs (**Figure 1a**). The timing of methylation establishment of one DMR (*FAM50B*-DMR) has not yet been determined. On the other hand, there were 20 matDMRs and 9 patDMRs. We investigated whether susceptibility to aberrant methylation differed for each type of DMR in *Kv*DMR1-LOM patients. *Kv*DMR1 itself, a gametic and matDMR, was excluded from this analysis. Several DMRs were mapped to certain imprinted domains, e.g., three DMRs in the *ARHI* domain and four in the *GNAS* domain. However, these DMRs differed by type, and aberrant methylations of these DMRs were not always linked. We also had previously found that DMRs in the *GNAS* domain were independently aberrantly methylated in hepatoblastoma.[20] Therefore, we decided to perform statistical analyses assuming the independence of each DMR.

We first compared gametic DMRs with somatic DMRs and found no significant difference in susceptibility ($P = 0.42$, Fisher's exact test; **Figure 2a**). *FAM50B*-DMR was excluded from this comparison. By contrast, matDMRs were aberrantly methylated more frequently than patDMRs ($P = 0.042$, Fisher's exact test; **Figure 2b**). In addition, among the aberrantly methylated DMRs, 12 showed LOM and 4 showed GOM. When we compared LOM with GOM, LOM preferentially occurred on matDMRs ($P = 0.050$, Fisher's exact test; **Figure 2c**). In this subanalysis, *GNASXL*-DMR was counted as having both GOM and LOM (**Figure 1a**). Furthermore, among the 12 DMRs with LOM, most of them (10) were gametic DMRs. These results suggest that matDMRs are susceptible to aberrant methylation and that gametic maternally methylated DMRs tend to be susceptible to LOM in *Kv*DMR1-LOM patients.

Biallelic expression of imprinted genes induced by aberrant methylation at their corresponding DMRs

We continued our investigation by determining whether allelic expression was associated with the methylation status of the corresponding DMR. We selected three genes (*ZDBF2*, *FAM50B*, and *GNAS1A*) expressed in lymphocytes.[25–27] In the case of *ZDBF2*, bisulfite sequencing of *ZDBF2*-DMR showed paternal monoallelic methylation in normal controls heterozygous for a specific SNP (*rs1861437*), whereas four BWS patients with GOM showed biallelic methylation: these findings were consistent with the results of MALDI-TOF MS and bisulfite pyrosequencing (**Figure 3a,b** and **Supplementary Figure S5** online). Because paternal expression of the *ZDBF2* gene is coupled with methylation of *ZDBF2*-DMR on the paternal allele,[25] biallelic expression due to biallelic methylation was expected. Indeed, three BWS patients heterozygous for a coding SNP (*rs10932150*) with hypermethylated DMRs clearly showed biallelic expression, in contrast with the paternal monoallelic expression in patients with normally methylated DMRs (**Figure 3c**). *FAM50B* and *GNAS1A* were paternally expressed and were coupled with maternal methylation of corresponding DMRs. RT-PCR using coding SNPs (*rs6597007* for *FAM50B* and *rs143800311* for *GNAS1A*) revealed that both genes were expressed biallelically with LOM of each corresponding DMR, which was in contrast with monoallelic expression in the patients with normally methylated DMRs (**Figure 4** and **Supplementary Figure S5** online). It is intriguing that *FAM50B* in patient BWS-s096 and *GNAS1A* in patient BWS-s062 were expressed from the maternal allele despite low-grade LOM,

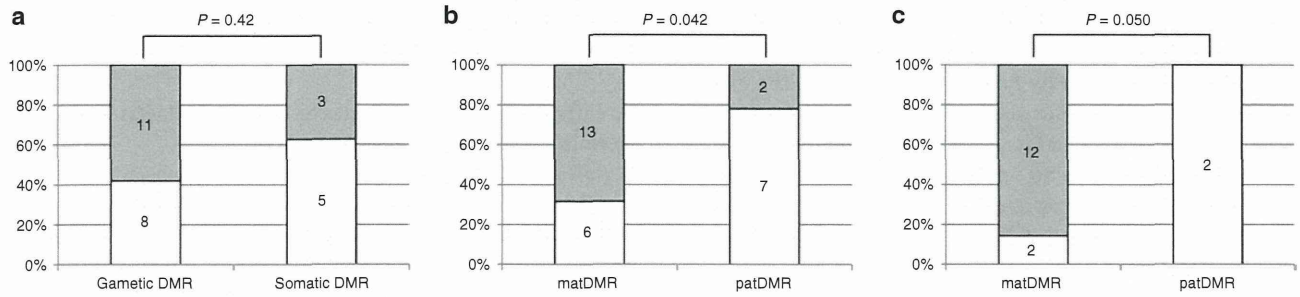

	Gametic DMR	Somatic DMR
Aberrant meth	11	3
Normal meth	8	5

	matDMR	patDMR
Aberrant meth	13	2
Normal meth	6	7

	matDMR	patDMR
LOM	12	0
GOM	2	2

Figure 2 Statistical analyses of aberrantly methylated differentially methylated region (DMRs). (**a**) Comparison of the number of aberrantly methylated DMRs between gametic DMRs and somatic DMRs in *Kv*DMR1-LOM patients. There was no statistical difference between the two DMRs ($P = 0.42$, Fisher's exact test). (**b**) Comparison of the number of aberrantly methylated DMRs between matDMRs and patDMRs in *Kv*DMR1-LOM patients. matDMRs were aberrantly methylated more frequently than patDMRs ($P = 0.042$, Fisher's exact test). (**c**) Comparison of the number of LOMs and GOMs between matDMRs and patDMRs among the aberrantly methylated DMRs in *Kv*DMR1-LOM patients. LOM preferentially occurred on matDMRs ($P = 0.050$, Fisher's exact test). GOM, gain of methylation; LOM, loss of methylation; matDMR, maternally methylated DMR; patDMR, paternally methylated DMR.

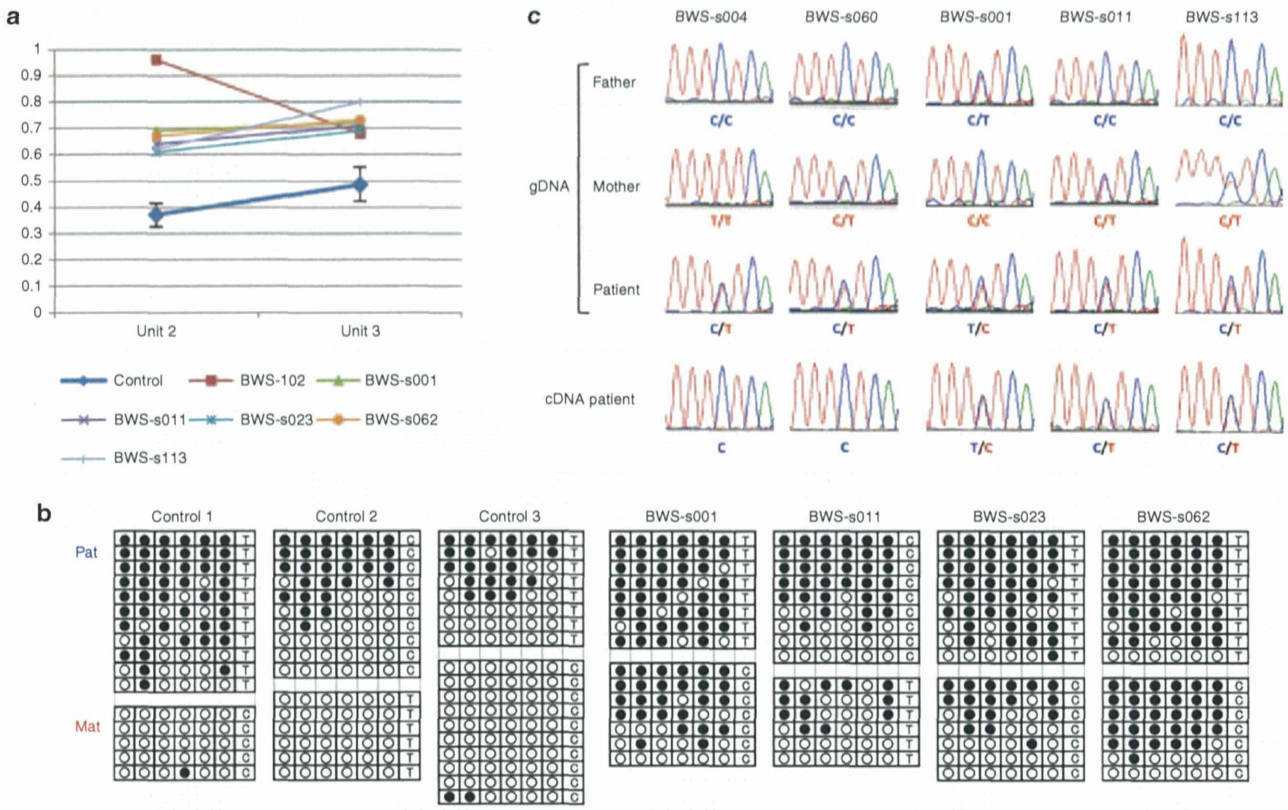

Figure 3 Methylation analysis of *ZDBF2*-DMR and expression analysis of the *ZDBF2* gene. (**a**) Results of matrix-assisted laser desorption/ionization mass spectrometry analysis. Averages with SD of 24 normal controls are shown in blue. Methylation indexes of the patients showing GOM are indicated in different colors. Units 1 and 2 included two and one CpG sites, respectively. (**b**) Results of bisulfite sequencing. Normal controls show monoallelic differential methylation, whereas four Beckwith–Wiedemann syndrome (BWS) patients (BWS-s001, BWS-s011, BWS-s023, and BWS-s060) show biallelic methylation. Two parental alleles were distinguished by a SNP (*rs1861437*). Mat, maternal allele; Pat, paternal allele. (**c**) Results of expression analysis of the *ZDBF2* gene. Three BWS patients (BWS-s001, BWS-s011, and BWS-s113) heterozygous for a coding SNP (*rs10932150*) with GOM clearly showed biallelic expression; by contrast, two patients with normally methylated differentially methylated region (DMRs) exhibited paternal monoallelic expression (patients BWS-s004 and BWS-s060). gDNA, genomic DNA; GOM, gain of methylation; SNP, single-nucleotide polymorphism.

which suggests that our definition of aberrant methylation is appropriate. In addition, we investigated the expression levels of *ZDBF2* and *FAM50B* by quantitative RT-PCR. The expression levels in patients with aberrantly methylated DMRs were higher than those in patients with normally methylated DMRs (**Supplementary Figure S6** online). These results indicate that allelic expression and expression levels were indeed associated with the methylation status of the corresponding DMR in patients with MMDs.

Lack of pathological variation in all aberrantly methylated DMRs in *Kv*DMR1-LOM patients

Because the genetic aberrations of *H19*DMR explained only ~20% of BWS patients with *H19*DMR-GOM,[28] we hypothesized the existence of *cis*-acting variations within aberrantly methylated DMRs. Therefore, we sequenced all aberrantly methylated DMRs, including *Kv*DMR1, in *Kv*DMR1-LOM patients. However, no variations were found in any aberrantly hypomethylated DMRs, except for four known SNPs (summarized in **Supplementary Figure S7** online), suggesting that *cis*-acting pathological variations are not involved in aberrant methylation of these DMRs.

No difference in clinical features between MMDs and monolocus methylation defects

In *Kv*DMR1-LOM patients, there was no significant difference in clinical features between MMDs and monolocus methylation defects, which demonstrated LOM only at *Kv*DMR1 (**Table 1**). Among 27 patients with *Kv*DMR1-LOM for whom information on conception was available, one patient was conceived using intracytoplasmic sperm injection, two were from artificial insemination by the husband, and two were from ovulation stimulation. We searched for a link between assisted reproductive technology and MMD but could find no relationship (**Table 1**). The average age of neither the mother nor the father differed between patients with MMDs versus those with monolocus methylation defects (**Table 1**). The fact that monozygotic twins discordant for BWS were found predominantly for females suggests an insufficient amount of DNA methyltransferase 1 (DNMT1) to maintain *Kv*DMR1 methylation during the overlap in timing

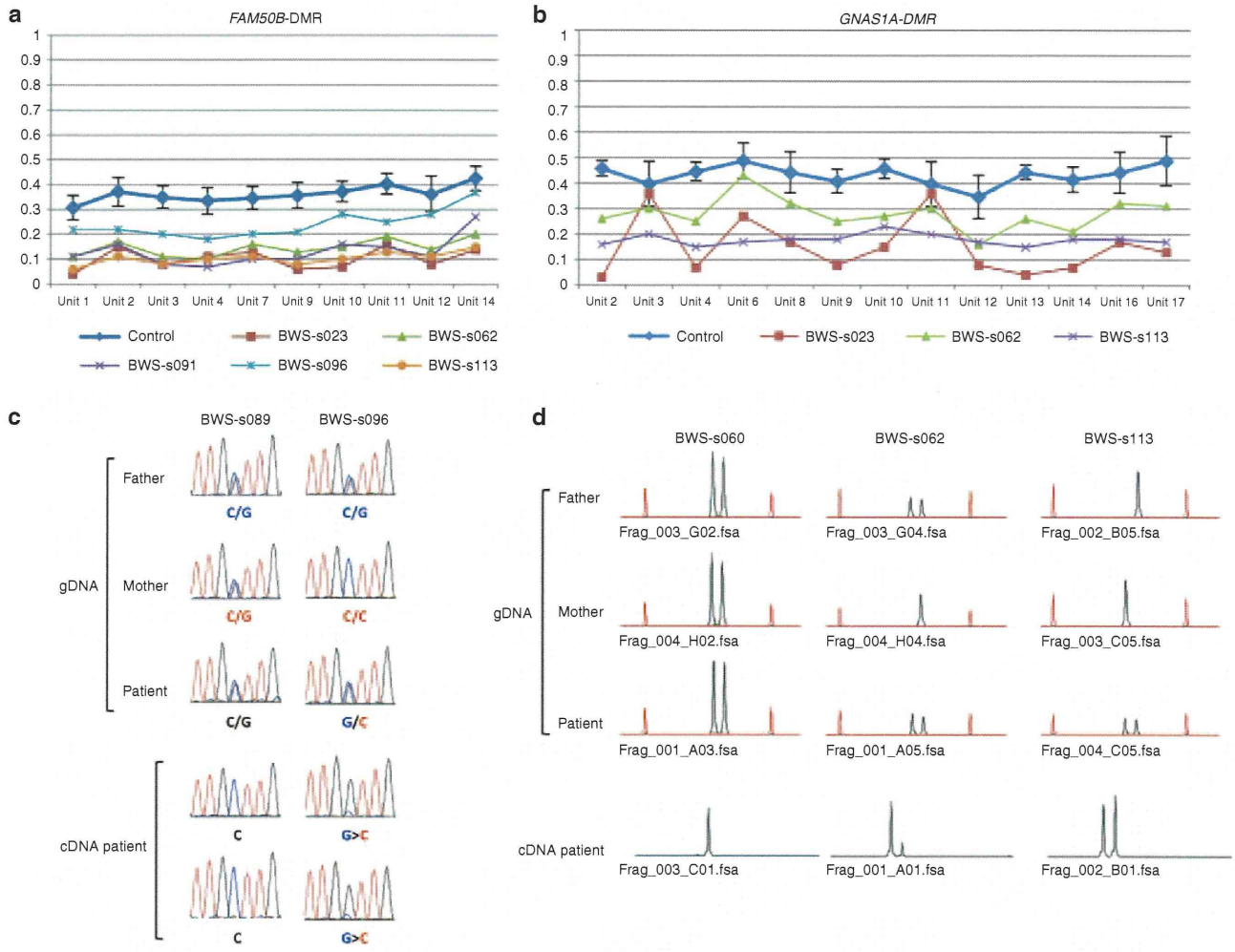

Figure 4 Methylation analysis of *FAM50*B- and *GNAS1A*-DMRs and expression analysis of the *FAM50*B and *GNAS1A* genes. (**a**,**b**) Results of matrix-assisted laser desorption/ionization mass spectrometry analysis. Averages with SD of 24 normal controls are shown in blue. Methylation indexes of patients showing LOM are indicated in different colors. Ten CpG units analyzed for *FAM50B*-DMR covered 13 CpG sites, and 13 CpG units analyzed for *GNAS1A*-DMR covered 18 CpG sites. (**c**) Results of expression analysis of the *FAM50B* gene. Beckwith–Wiedemann syndrome (BWS) patient BWS-s096 was heterozygous for a coding SNP (*rs6597007*) with LOM and showed biallelic expression with a low peak of maternal expression, whereas monoallelic expression was seen in a patient with normally methylated differentially methylated regions (DMRs) (patient BWS-s089). In patient BWS-s096, maternal expression was noted in two independent analyses despite low-grade LOM. gDNA, genomic DNA. (**d**) Results of expression analysis of the *GNAS1A* gene. Patients BWS-s062 and BWS-s113, heterozygous for a deletion/insertion variation (*rs143800311*) with LOM, showed biallelic expression, whereas patient BWS-s060 possessed normally methylated DMRs and exhibited monoallelic expression. Maternal expression was noted despite low-grade LOM in patient BWS-s062. Red peaks are molecular markers. GOM, gain of methylation; LOM, loss of methylation.

with X-chromosome inactivation and twinning.[29] This hypothesis suggests that females might tend to suffer from MMDs. We compared the frequency of female patients with MMDs with the frequency of those with monolocus methylation defects, but no significant difference could be found (**Table 1**).

DISCUSSION

Currently, most reports have studied 3–10 imprinted DMRs in BWS patients,[7–10,13] with the exception of two reports in which 16 and 27 DMRs were analyzed.[11,12] In addition, the quantitative capability of methods used for multiple methylation analyses has been variable, and few studies have conducted multiple checks to confirm the methylation statuses of all DMRs showing aberrant methylation.[7–13] To resolve these matters, we analyzed 29 DMRs and confirmed all aberrantly methylated DMRs using MALDI-TOF MS and bisulfite pyrosequencing, which are the most reliable quantitative methods of methylation analysis available at present.[19,30,31] We found that 34.1% of *Kv*DMR1-LOM patients exhibited MMDs. The frequency was higher than that in previous reports, which can be summarized as reporting an overall frequency of 20.6% (102 of 495 patients).[7–13] However, within these reports, the frequency in studies that analyzed 10 or fewer DMRs is 19.0% (82 of 431),[7–10,13] and the frequency in studies that analyzed more than 10 DMRs is 31.3% (20 of

Table 1 Clinical features of *Kv*DMR-LOM patients with monolocus methylation defect and those with multilocus methylation defects

	Methylation defect		
	Monolocus	**Multilocus**	***P* value**
Sex			0.22
Male	15	5	
Female	13	9	
Average age of patients	3.3	2.4	0.098[a]
Average age of parents			
Father	31.8	33.8	0.93[a]
Mother	31.8	30.3	0.37[a]
Assisted reproduction technology	3/19 (20%) (AIH 2, OS 1)	2/8 (29%) (ICSI 1, OS 1)	0.47
Standard deviation of average birth weight	+1.9	+2.0	0.58[a]
Overgrowth	21/28 (75%)	9/13 (69%)	0.78
Abdominal wall defect	22/29 (76%)	12/13 (92%)	0.21
Macroglossia	29/29 (100%)	12/12 (100%)	0.60
Hypoglycemia	14/27 (52%)	5/12 (42%)	0.41
Ear pits and creases	19/27 (70.4%)	8/12 (67%)	0.73
Nevus flammeus	9/26 (35%)	4/10 (40%)	0.53
Hemihypertrophy	6/27 (22%)	6/13 (46%)	0.12
Renal anomaly	2/26 (8%)	0/11 (0%)	0.49
Renal enlargement	6/28 (21%)	1/13 (8%)	0.27
Adrenal enlargement	1/27 (4%)	0/11 (0%)	0.71
Hepatomegaly	5/29 (17%)	2/12 (17%)	0.67
Splenomegaly	6/29 (21%)	2/12 (17%)	0.57
Abnormal external genitalia	2/28 (7%)	0/12 (0%)	0.49
Increased bone age	2/15 (13%)	0/3 (0%)	0.69
Cardiac anomaly	2/23 (9%)	0/11 (0%)	0.82
Developmental retardation	6/22 (27%)	0/9 (0%)	0.10
Childhood tumor	5/26 (19%)	0/11 (0%)	0.15

AIH, artificial insemination by husband; ICSI, intracytoplasmic sperm injection; LOM, loss of methylation; OS, ovulation stimulation.

[a]Mann–Whitney *U*-test. Fisher's exact test was used for other analyses.

64).[11,12] In addition, we found that 30.0% of *H19*DMR-GOM patients showed MMDs, which is surprising considering that no MMDs were found in two previous reports in which 10 and 16 DMRs were analyzed.[8,11] These data suggest that the greater the number of DMRs analyzed, the higher the frequency of MMDs observed. In future, all DMRs in the genome should be analyzed to understand the precise frequency of MMDs, which DMRs become preferentially aberrantly methylated, and the mechanism by which MMDs occur.

In both *Kv*DMR1-LOM patients and *H19*DMR-GOM patients, we found MMDs in which not only LOM but also GOM were seen. We also found that both matDMRs and patDMRs were aberrantly methylated in both patient groups. It is noteworthy that matDMRs, probably gametic maternally methylated DMRs, were more susceptible to aberrant methylation than patDMRs in *Kv*DMR1-LOM patients, although no particular parent-based pattern of aberrant methylation has been reported previously.[12] This suggests that gametic maternally methylated DMRs are vulnerable to DNA demethylation during the preimplantation stage of early embryogenesis when *Kv*DMR1-LOM occurs.

Although it has not been reported that aberrant methylation of the corresponding DMR affects imprinted gene expression in MMD patients, we found biallelic expression of three imprinted genes (*ZDBF2*, *FAM50B*, and *GNAS1A*) to be associated with the aberrant methylation of their respective DMRs. Because biallelic expression increased the total expression levels of *ZDBF2* and *FAM50B*, we expect that had we measured the expression levels of *GNAS1A*, we would have observed an increase. Therefore, alteration of gene expression levels due to MMDs might affect the phenotype; however, clinical features between MMDs and monolocus methylation defects were not different in our study. This lack of difference has been previously reported,[7,9,10,13] although a few groups have reported a

difference in clinical features.[8,11,12] Two reasons for this similarity in terms of clinical features could be suggested. First, the mosaic ratio might be different in each organ. Because aberrant methylation was generally partial, it would occur after fertilization, and the patients would be mosaic. A high mosaic ratio would be a critical factor in the emergence of a distinct phenotype in BWS patients with monolocus methylation defects. Second, the imprinted locus at 11p15 might be epidominant over other imprinted loci because all MMD patients were clinically diagnosed as BWS.

Regarding the causative factor(s) for MMD, we could not find any pathological variation in any aberrantly methylated DMR, including *Kv*DMR1, suggesting that *cis*-acting variations of each specific DMR itself were not involved in the genesis of MMDs. On the other hand, the involvement of *trans*-acting factors has been advocated in other reports because mutations of *ZFP57* (which are required for the postfertilization maintenance of maternal and paternal methylation imprinting at multiple loci) have been found in transient neonatal diabetes mellitus type 1 patients with multilocus hypomethylation.[32] Mutations of *NLRP2* were also identified in a BWS patient with *Kv*DMR1-LOM and *MEST*-LOM in a family with complex consanguinity and in a Silver–Russell syndrome patient with multilocus hypomethylation.[12,33] In addition, TRIM28, NLRP7, KHDC3L, and DNMT3L have been considered to be candidate *trans*-acting factors. However, no mutations in any of these candidates or other genes, such as *DNMT1*, *DNMT3A*, and *DNMT3B*, were found in our BWS patients with MMDs, as determined by exome sequencing (K. Sasaki and K. Hata, personal communication). Recently, Lorthongpanich et al.[34] reported that the absence of maternal *Trim28* until zygotic gene activation at the two-cell late stage caused mosaicism of MMDs randomly, suggesting that insufficient expression of the candidate gene(s) at very early embryogenesis is an important event in the generation of MMDs in human imprinted diseases. Whole-genome sequencing and whole-genome bisulfite sequencing, including the regulatory regions of the candidate genes, and transcriptome analysis in early embryogenesis would be useful to identify the cause(s) of MMDs.

In our *H19*DMR-GOM patients, we also found GOM of *IGF2*-DMR0 and *IGF2*-DMR2 to be associated with GOM of *H19*DMR and *H19promoter* DMR, in agreement with previous reports.[22,35,36] Two patients showed simultaneous GOM at both *IGF2*-DMRs. Because *Igf2*-DMRs were established at the postimplantation stage under the control of *H19*DMR in mice,[37] GOM of *IGF2*-DMRs in BWS is likely to occur at the same stage. Although the function of *IGF2*-DMR0 is still unknown, methylated *Igf2*-DMR2 plays a role in transcription initiation of *Igf2* in mice.[38] GOM of the DMRs might change the high-order chromatin structure of the maternal allele and increase the expression of *IGF2* in cooperation with *H19*DMR-GOM in BWS patients.

In conclusion, our comprehensive and quantitative methylation analysis of multiple imprinted DMRs revealed several new findings: (i) matDMRs, probably gametic maternally methylated DMRs, are more susceptible to aberrant methylation during the preimplantation stage, when *Kv*DMR1-LOM occurs; (ii) aberrant methylation indeed alters imprinted gene expression; and (iii) *cis*-acting pathological variations of each DMR are not involved in the MMDs analyzed. Moreover, our study confirmed the simultaneous aberrant hypermethylation of *IGF2*-DMR0 and/or -DMR2 with isolated *H19*DMR-GOM. These findings may help us to understand the molecular mechanisms and pathophysiological features of MMDs.

SUPPLEMENTARY MATERIAL

Supplementary material is linked in the online version of the paper at http://www.nature.com/gim.

ACKNOWLEDGMENTS

We thank all the participants and their families who provided samples and all the doctors who referred patients to us. This study was supported, in part, by a Grant for Research on Intractable Diseases from the Ministry of Health, Labor, and Welfare; a Grant for Child Health and Development from the National Center for Child Health and Development; a Grant-in-Aid for Challenging Exploratory Research; and a Grant-in-Aid for Scientific Research (C) from the Japan Society for the Promotion of Science.

DISCLOSURE

The authors declare no conflict of interest.

REFERENCES

1. Abramowitz LK, Bartolomei MS. Genomic imprinting: recognition and marking of imprinted loci. *Curr Opin Genet Dev* 2012;22:72–78.
2. Tomizawa S, Sasaki H. Genomic imprinting and its relevance to congenital disease, infertility, molar pregnancy and induced pluripotent stem cell. *J Hum Genet* 2012;57:84–91.
3. Weksberg R, Shuman C, Beckwith JB. Beckwith-Wiedemann syndrome. *Eur J Hum Genet* 2010;18:8–14.
4. Choufani S, Shuman C, Weksberg R. Beckwith-Wiedemann syndrome. *Am J Med Genet C Semin Med Genet* 2010;154C:343–354.
5. Soejima H, Higashimoto K. Epigenetic and genetic alterations of the imprinting disorder Beckwith-Wiedemann syndrome and related disorders. *J Hum Genet* 2013;58:402–409.
6. Mackay DJ, Boonen SE, Clayton-Smith J, et al. A maternal hypomethylation syndrome presenting as transient neonatal diabetes mellitus. *Hum Genet* 2006;120:262–269.
7. Rossignol S, Steunou V, Chalas C, et al. The epigenetic imprinting defect of patients with Beckwith-Wiedemann syndrome born after assisted reproductive technology is not restricted to the 11p15 region. *J Med Genet* 2006;43:902–907.
8. Bliek J, Verde G, Callaway J, et al. Hypomethylation at multiple maternally methylated imprinted regions including PLAGL1 and GNAS loci in Beckwith-Wiedemann syndrome. *Eur J Hum Genet* 2009;17:611–619.
9. Azzi S, Rossignol S, Steunou V, et al. Multilocus methylation analysis in a large cohort of 11p15-related foetal growth disorders (Russell Silver and Beckwith Wiedemann syndromes) reveals simultaneous loss of methylation at paternal and maternal imprinted loci. *Hum Mol Genet* 2009;18:4724–4733.
10. Lim D, Bowdin SC, Tee L, et al. Clinical and molecular genetic features of Beckwith-Wiedemann syndrome associated with assisted reproductive technologies. *Hum Reprod* 2009;24:741–747.
11. Poole RL, Docherty LE, Al Sayegh A, et al.; International Clinical Imprinting Consortium. Targeted methylation testing of a patient cohort broadens the epigenetic and clinical description of imprinting disorders. *Am J Med Genet A* 2013;161:2174–2182.
12. Court F, Martin-Trujillo A, Romanelli V, et al. Genome-wide allelic methylation analysis reveals disease-specific susceptibility to multiple methylation defects in imprinting syndromes. *Hum Mutat* 2013;34:595–602.

13. Tee L, Lim DH, Dias RP, et al. Epimutation profiling in Beckwith-Wiedemann syndrome: relationship with assisted reproductive technology. *Clin Epigenetics* 2013;5:23.
14. DeBaun MR, Tucker MA. Risk of cancer during the first four years of life in children from The Beckwith-Wiedemann Syndrome Registry. *J Pediatr* 1998;132(3 Pt 1):398–400.
15. Soejima H, Nakagawachi T, Zhao W, et al. Silencing of imprinted CDKN1C gene expression is associated with loss of CpG and histone H3 lysine 9 methylation at DMR-LIT1 in esophageal cancer. *Oncogene* 2004;23:4380–4388.
16. Higashimoto K, Nakabayashi K, Yatsuki H, et al. Aberrant methylation of H19-DMR acquired after implantation was dissimilar in soma versus placenta of patients with Beckwith-Wiedemann syndrome. *Am J Med Genet A* 2012;158A:1670–1675.
17. Yatsuki H, Higashimoto K, Jozaki K, et al. Novel mutations of CDKN1C in Japanese patients with Beckwith-Wiedemann syndrome. *Genes & Genomics* 2013;35:141–147.
18. Higashimoto K, Jozaki K, Kosho T, et al. A novel de novo point mutation of the OCT-binding site in the IGF2/H19-imprinting control region in a Beckwith-Wiedemann syndrome patient. *Clin Genet* 2013; e-pub ahead of print 8 November 2013.
19. Ehrich M, Nelson MR, Stanssens P, et al. Quantitative high-throughput analysis of DNA methylation patterns by base-specific cleavage and mass spectrometry. *Proc Natl Acad Sci USA* 2005;102:15785–15790.
20. Rumbajan JM, Maeda T, Souzaki R, et al. Comprehensive analyses of imprinted differentially methylated regions reveal epigenetic and genetic characteristics in hepatoblastoma. *BMC Cancer* 2013;13:608.
21. Cui H, Onyango P, Brandenburg S, Wu Y, Hsieh CL, Feinberg AP. Loss of imprinting in colorectal cancer linked to hypomethylation of H19 and IGF2. *Cancer Res* 2002;62:6442–6446.
22. Murrell A, Ito Y, Verde G, et al. Distinct methylation changes at the IGF2-H19 locus in congenital growth disorders and cancer. *PLoS One* 2008;3: e1849.
23. Woodfine K, Huddleston JE, Murrell A. Quantitative analysis of DNA methylation at all human imprinted regions reveals preservation of epigenetic stability in adult somatic tissue. *Epigenetics Chromatin* 2011;4:1.
24. Reik W, Maher ER. Imprinting in clusters: lessons from Beckwith-Wiedemann syndrome. *Trends Genet* 1997;13:330–334.
25. Kobayashi H, Yamada K, Morita S, et al. Identification of the mouse paternally expressed imprinted gene Zdbf2 on chromosome 1 and its imprinted human homolog ZDBF2 on chromosome 2. *Genomics* 2009;93:461–472.
26. Nakabayashi K, Trujillo AM, Tayama C, et al. Methylation screening of reciprocal genome-wide UPDs identifies novel human-specific imprinted genes. *Hum Mol Genet* 2011;20:3188–3197.
27. Liu J, Litman D, Rosenberg MJ, Yu S, Biesecker LG, Weinstein LS. A GNAS1 imprinting defect in pseudohypoparathyroidism type IB. *J Clin Invest* 2000;106:1167–1174.
28. Demars J, Shmela ME, Rossignol S, et al. Analysis of the IGF2/H19 imprinting control region uncovers new genetic defects, including mutations of OCT-binding sequences, in patients with 11p15 fetal growth disorders. *Hum Mol Genet* 2010;19:803–814.
29. Weksberg R, Shuman C, Caluseriu O, et al. Discordant KCNQ1OT1 imprinting in sets of monozygotic twins discordant for Beckwith-Wiedemann syndrome. *Hum Mol Genet* 2002;11:1317–1325.
30. Tost J, Dunker J, Gut IG. Analysis and quantification of multiple methylation variable positions in CpG islands by Pyrosequencing. *Biotechniques* 2003;35:152–156.
31. Claus R, Wilop S, Hielscher T, et al. A systematic comparison of quantitative high-resolution DNA methylation analysis and methylation-specific PCR. *Epigenetics* 2012;7:772–780.
32. Mackay DJ, Callaway JL, Marks SM, et al. Hypomethylation of multiple imprinted loci in individuals with transient neonatal diabetes is associated with mutations in ZFP57. *Nat Genet* 2008;40:949–951.
33. Meyer E, Lim D, Pasha S, et al. Germline mutation in NLRP2 (NALP2) in a familial imprinting disorder (Beckwith-Wiedemann Syndrome). *PLoS Genet* 2009;5:e1000423.
34. Lorthongpanich C, Cheow LF, Balu S, et al. Single-cell DNA-methylation analysis reveals epigenetic chimerism in preimplantation embryos. *Science* 2013;341:1110–1112.
35. Reik W, Brown KW, Schneid H, Le Bouc Y, Bickmore W, Maher ER. Imprinting mutations in the Beckwith-Wiedemann syndrome suggested by altered imprinting pattern in the IGF2-H19 domain. *Hum Mol Genet* 1995;4:2379–2385.
36. Sparago A, Russo S, Cerrato F, et al. Mechanisms causing imprinting defects in familial Beckwith-Wiedemann syndrome with Wilms' tumour. *Hum Mol Genet* 2007;16:254–264.
37. Lopes S, Lewis A, Hajkova P, et al. Epigenetic modifications in an imprinting cluster are controlled by a hierarchy of DMRs suggesting long-range chromatin interactions. *Hum Mol Genet* 2003;12:295–305.
38. Murrell A, Heeson S, Bowden L, et al. An intragenic methylated region in the imprinted Igf2 gene augments transcription. *EMBO Rep* 2001;2:1101–1106.